Endoglycan plays a role in axon guidance and neuronal migration by negatively regulating cell-cell adhesion

Thomas Baeriswyl*, Alexandre Dumoulin*, Martina Schaettin*, Georgia Tsapara*, Vera Niederkofler, Denise Helbling, Evelyn Avilés, Jeannine A. Frei, Nicole H. Wilson, Matthias Gesemann, and Esther T. Stoeckli[1]

Department of Molecular Life Sciences and Neuroscience Center Zurich, University of Zurich, Winterthurerstrasse 190, 8057 Zurich, Switzerland

phone: +41 44 635 4840
e-mail: esther.stoeckli@mls.uzh.ch

[1] corresponding author
[*] T.B., A.D., M.S., and G.T. contributed equally to this study

short title: Endoglycan in axon guidance and cell migration

Key words: sialomucin, commissural axons, Purkinje cells, ex ovo RNAi, floor plate, cell migration, Podocalyxin-like 2, live imaging

SUMMARY

Cell migration and axon guidance are important steps in the formation of neural circuits. Both steps depend on the interactions between cell surface receptors and molecules on cells along the pathway. In addition to cell-cell adhesion, these molecular interactions provide guidance information. The fine-tuning of cell-cell adhesion is an important aspect of cell migration, axon guidance, and synapse formation.

Here, we show that Endoglycan, a sialomucin, plays a role in axon guidance and cell migration in the central nervous system. In the absence of Endoglycan, commissural axons failed to properly navigate the midline of the spinal cord. In the developing cerebellum, a lack of Endoglycan prevented migration of Purkinje cells and resulted in a stunted growth of the cerebellar lobes. Taken together, these results support the hypothesis that Endoglycan acts as a 'lubricant', a negative regulator of cell-cell adhesion, in both commissural axon guidance and Purkinje cell migration.

INTRODUCTION

Cell migration and axonal pathfinding are crucial aspects of neural development. Neurons are born in proliferative zones from where they migrate to their final destination. After their arrival, they send out axons that have to navigate through the tissue to find the target cells with which they establish synaptic contacts. Intuitively, it is clear that the same cues provided by the environment can guide both cells and axons to their target. Although we know relatively little about guidance cues for cells compared to guidance cues for axons, both processes are dependent on proper cell-cell contacts (Gomez and Letourneau, 2014; Short et al., 2016).

One of the best-studied model systems for axon guidance are the commissural neurons located in the dorsolateral spinal cord (de Ramon Francàs et al., 2017; Stoeckli, 2017 and 2018). These neurons send out their axons toward the ventral midline under the influence of the roof plate-derived repellents BMP7 (Augsburger et al., 1999) and Draxin (Islam et al., 2009). At the same time, axons are attracted to the floor plate, their intermediate target, by Netrin (for a review on Netrin function, see Boyer and Gupton, 2018), VEGF (Ruiz de Almodóvar et al., 2011), and Shh (Yam et al., 2009 and 2012). At the floor-plate border, commissural axons require the short-range guidance cues Contactin2 (aka Axonin-1) and NrCAM to enter the midline area (Stoeckli

and Landmesser, 1995; Stoeckli et al., 1997; Fitzli et al., 2000; Pekarik et al., 2003). Slits and their receptors, the Robos, were shown to be required as negative signals involved in pushing axons out of the midline area (Long et al., 2004; Blockus and Chédotal, 2016). Members of the Semaphorin family are also involved in midline crossing either as negative signals mediated by Neuropilin-2 (Zou et al., 2000; Parra and Zou, 2010; Nawabi et al., 2010; Charoy et al., 2012) or as receptors for floor-plate derived PlexinA2 (Andermatt et al., 2014a). Once commissural axons exit the floor-plate area, they turn rostrally along the longitudinal axis of the spinal cord. Morphogens of the Wnt family (Lyuksyutova et al., 2003; Domanitskaya et al., 2010; Avilés and Stoeckli, 2016) and Shh (Bourikas et al., 2005; Wilson and Stoeckli, 2013) were identified as guidance cues directing post-crossing commissural axons rostrally. In the same screen that resulted in the discovery of Shh as a repellent for post-crossing commissural axons (Bourikas et al., 2005), we found another candidate that interfered with the rostral turn of post-crossing commissural axons. This candidate gene was identified as *Endoglycan*.

Endoglycan is a member of the CD34 family of sialomucins (Nielsen and McNagny, 2008; Sassetti et al., 2000; Furness and McNagny, 2006). The family includes CD34, Podocalyxin (also known as Thrombomucin, PCLP-1, MEP21, or gp135), and Endoglycan (also known as Podocalyxin-like 2). They are single-pass transmembrane proteins with highly conserved transmembrane and cytoplasmic domains. A C-terminal PDZ recognition site is found in all three family members (Furness and McNagny, 2006; Nielsen and McNagny, 2008). The hallmark of sialomucins is their bulky extracellular domain that is negatively charged due to extensive N- and O-glycosylation. Despite the fact that CD34 was identified more than 20 years ago, very little is known about its function. It has been widely used as a marker for hematopoietic stem cells and precursors. Similarly, Podocalyxin is expressed on hematopoietic stem and precursor cells. In contrast to CD34, Podocalyxin was found in podocytes of the developing kidney (Kerjaschki et al., 1984; Doyonnas et al., 2005; Furness and McNagny, 2006). In the absence of Podocalyxin, podocytes do not differentiate, resulting in kidney failure and thus perinatal lethality in mice (Doyonnas et al., 2001). *Podocalyxin*, but not *CD34*, is expressed widely in the developing and mature mouse brain (Vitureira et al., 2005; Vitureira et al., 2010). Podocalyxin was shown to induce microvilli and regulate cell-cell adhesion via its binding to the NHERF (Na^+/H^+ exchanger regulatory factor) family of adaptor proteins that link Podocalyxin to the actin cytoskeleton (Nielsen et al., 2007; Nielsen and McNagny, 2008; Nielsen and McNagny, 2009). Like *Podocalyxin*, *Endoglycan* is expressed in the brain and

in the kidney. Only low levels were found in hematopoietic tissues (Sassetti et al., 2000). To date, nothing is known about the function of Endoglycan.

Based on its temporal and spatial expression pattern, we first analyzed the function of Endoglycan in the embryonic chicken spinal cord. In the absence of Endoglycan commissural axons failed to turn rostrally upon floor-plate exit. Occasionally, they were observed to turn already inside the floor-plate area. Furthermore, the trajectory of commissural axons in the midline area was tortuous in embryos lacking Endoglycan, but straight in control embryos. Live imaging data of dI1 axons crossing the floor plate confirmed changes in axon – floor plate interaction. In addition, axons were growing more slowly after silencing *Endoglycan* and faster after overexpression of *Endoglycan*.

In the cerebellum, *Endoglycan* expression is restricted to migrating Purkinje cells. The absence of Endoglycan resulted in the failure of Purkinje cells to migrate properly from the ventricular zone to their destination in the periphery of the cerebellum, where they normally form the typical Purkinje cell layer. This in turn resulted in a decrease in granule cell proliferation and in the stunted growth of the cerebellar folds.

Taken together, our results from in vitro and in vivo studies along with live imaging observations are consistent with a role for Endoglycan as a 'lubricant', a negative regulator of cell-cell contact and therefore modulator of molecular interactions affecting both axon guidance and cell migration.

RESULTS

Endoglycan was identified as a candidate guidance cue for commissural axons

In a subtractive hybridization screen, we identified differentially expressed floor-plate genes as candidate guidance cues directing axons from dorsolateral commissural neurons (dI1 neurons) along the longitudinal axis after midline crossing (Bourikas et al., 2005; see Methods). Candidates with an expression pattern that was compatible with a role in commissural axon navigation at the midline were selected for functional analysis using in ovo RNAi (Pekarik et al., 2003; Wilson and Stoeckli, 2011). One of these candidates that interfered with

113 the correct rostral turning of commissural axons after midline crossing turned out to be *Endoglycan*, a member
114 of the CD34 family of sialomucins.
115 CD34 family members share a common domain organization that consists of a mucin-like domain followed by a
116 cysteine-containing globular domain, a membrane associated stalk region, a transmembrane spanning domain
117 and the cytoplasmic domain (Supplementary Figure 1; Sassetti et al., 2000; Furness and McNagny, 2006;
118 Nielsen and McNagny, 2008). With the exception of the mucin-like domain at the N-terminus, the conservation
119 between species orthologues of CD34, Endoglycan and Podocalyxin is in the range of 80%, but drops below
120 40% within the mucin domain. However, homologies of these paralogous proteins within the same species are
121 generally only in the range of 40% (Supplementary Figure 1), demonstrating that, while they might share a
122 similar overall structure, the structure can be built by quite diverse primary amino acid sequences.
123
124 *Endoglycan* was expressed mainly in the nervous system during development, as levels in non-neuronal tissues
125 were much lower (Supplementary Figure 2). In the neural tube, *Endoglycan* was expressed ubiquitously
126 including floor-plate cells at HH21 (Hamburger and Hamilton stage 21; Hamburger and Hamilton, 1951; Figure
127 1). By HH25, expression was still found throughout the neural tube withhigher levels detected in dorsal
128 neurons (including dI1 neurons) and motoneurons. *Endoglycan* expression was also maintained in the floor
129 plate (Figure 1B). For functional analysis, dsRNA was produced from the *Endoglycan* cDNA fragment obtained
130 from a screen and used for in ovo electroporation of the spinal cord at HH18 (Figure 1D). The analysis of
131 commissural axons' trajectories at HH26 by DiI tracing in „open-book" preparations (Figure 1E; quantified in
132 Figure 1L) revealed either failure to turn or erroneous caudal turns along the contralateral floor-plate border in
133 embryos lacking Endoglycan in the floor plate (Figure 1G), in only the dorsal spinal cord (Figure 1J), or in one
134 half of the spinal cord including the floor plate (Figure 1H,I). Furthermore, axons were occasionally found to
135 turn prematurely either before midline crossing or within the floor-plate area. Detailed analysis of the axonal
136 morphology in the floor-plate area revealed a tortuous, 'corkscrew'-like trajectory in embryos lacking
137 Endoglycan in dI1 neurons and the floor plate (Figure 1I), whereas axons crossed the midline in a straight
138 trajectory in untreated control embryos (Figure 1F) and in embryos injected and electroporated with dsRNA
139 derived from either CD34 (not shown) or Podocalyxin (Figure 1K).
140 To demonstrate specificity of Endoglycan downregulation and to verify that the phenotype was not due to an
141 off-target effect, we used three non-overlapping cDNA fragments to produce dsRNA. All fragments resulted in

142 the same phenotypes. Downregulation of Endoglycan with dsRNA derived from the ORF resulted in 61.7±6.4%
143 injection sites with aberrant axon guidance. The effect on axon guidance was also seen with dsRNA derived
144 from the 3'UTR, with 82.3±5.6% of the injection sites with aberrant axon guidance (Figure 1L). In contrast,
145 aberrant axonal pathfinding was seen only at 6.7±3.4% of the injection sites in untreated control embryos.
146 Values were 16.2±6.0 for EGFP-expressing control embryos, 24.6±5.8% for embryos transfected with dsRNA
147 derived from *CD34*, and 23.3±3.9% for embryos transfected with dsRNA derived from *Podocalyxin*. Thus,
148 silencing either *CD34* or *Podocalyxin* did not interfere with correct navigation of axons at the midline. Because
149 both of them were expressed in the developing spinal cord (Supplementary Figure 3), these results further
150 support the specificity of the observed effects of *Endoglycan* silencing.
151
152
153 **Lack of Endoglycan affects the morphology of the floor plate only after dI1 axons have crossed the midline**
154
155 Because the hallmark of sialomucins is their bulky, negatively charged extracellular domain with extensive
156 glycosylation, a role as regulators of cell-cell adhesion has been postulated (Vitureira et al., 2010; Takeda et al.,
157 2000; Nielsen and McNagny, 2008 and 2009). This together with our observation that commissural axons have
158 a „corkscrew"-like phenotype in the midline area in Endoglycan-deficient embryos prompted us to analyze the
159 morphology of the floor plate. Sections were taken from the lumbar level of the spinal cord at HH26 from
160 control-treated and experimental embryos and stained for HNF3β/FoxA2 to label floor-plate cells, and for
161 Contactin2 (aka Axonin-1) to label commissural axons (Figure 2). In untreated (Figure 2A-C) and control-treated
162 embryos (Figure 2D-F), HNF3β/FoxA2-positive cells were aligned to form the characteristic triangular shape of
163 the floor plate. In particular, the ventral border of the floor plate, where commissural axons traverse the
164 midline was smooth, because all floor-plate cells were precisely aligned (Figure 2A,D). In contrast, floor-plate
165 cells were no longer aligned to form a smooth ventral border in embryos lacking Endoglycan (Figure 2G,J). On
166 the one hand, floor-plate cells were found dislocated into the commissure formed by the Contactin2-positive
167 axons (arrowheads in Figure 2I,L). On the other hand, the floor plate appeared to have gaps in embryos lacking
168 Endoglycan. In addition, the floor-plate width was significantly narrower in embryos lacking Endoglycan in
169 comparison to age-matched controls (Figure 2S,T). These changes in floor-plate morphology were not due to
170 differences in cell differentiation or patterning (Supplementary Figure 4). Furthermore, we can exclude cell

171 death as a contributor to the changes in the floor plate, as we found no Cleaved Caspase-3-positive floor-plate
172 cells in any of the conditions.
173
174 When embryos lacking Endoglycan were analyzed at HH21 (Figure 2P-R), that is at a time point when dI1 axons
175 have reached but not yet crossed the floor plate, the morphology and the width of the floor plate were not
176 different from controls (Figure 2M-O). In contrast to measurements of floor-plate width at HH25 (Figure 2T),
177 the values for experimental and control embryos were not different at HH21 (Figure 2V). Thus, we concluded
178 that the absence of Endoglycan did not affect primarily cell-cell adhesion between floor-plate cells. Rather the
179 altered floor-plate morphology appeared to be an indirect effect of changes in axon to floor-plate adhesion.
180 We ruled out an effect of the perturbation of Endoglycan levels on the expression of known guidance cues of
181 dI1 axons, such as Contactin2 (Axonin-1) or NrCAM (Supplementary Figure 5). Similarly, we did not find changes
182 in the expression of Shh and Wnt5a, morphogens that are known to direct post-crossing dI1 axons rostrally
183 (Supplementary Figure 6; Bourikas et al., 2005; Lyuksyutova et al., 2003).
184
185 An alternative way of demonstrating the requirement for Endoglycan in both floor plate and commissural
186 axons were rescue experiments (Figure 3). We used dsRNA derived from the 3'-UTR and expressed the ORF of
187 *Endoglycan* either under control of the Math1 enhancer (expression only in dI1 neurons) or the Hoxa1
188 enhancer for floor-plate specific expression. Because expression of these plasmids in control embryos
189 (overexpression) resulted in aberrant behavior of axons at the floor plate, we used three different
190 concentrations of plasmid for our rescue experiments and obtained a dose-dependent effect on axon guidance.
191 Expression of high doses of *Endoglycan* was never able to rescue the axon guidance phenotype. However, axon
192 guidance was not different from control embryos after transfection of dI1 neurons with a low concentration or
193 floor-plate cells with a medium concentration of the *Endoglycan* ORF (Figure 3B; Table 1). Interestingly, the
194 source of Endoglycan did not matter but the amount of Endoglycan did. These findings were consistent with
195 the idea that Endoglycan was regulating adhesion, as both too much but also too little adhesion would be a
196 problem for axonal navigation. Furthermore, these results suggested that Endoglycan did not act as a receptor.
197
198
199 **Endoglycan is a negative regulator of cell adhesion**

200

201 The observation that downregulation of Endoglycan seemed to increase the adhesion between commissural
202 axons and floor-plate cells, together with the knowledge about its molecular features, led us to hypothesize
203 that Endoglycan might act as a negative regulator of cell-cell adhesion. As a first test, we counted the number
204 of motoneurons that adhered to a carpet of HEK cells stably expressing Endoglycan compared to control HEK
205 cells (Figure 4). Expression of Endoglycan interfered strongly with motoneuron adhesion, as the number of cells
206 was almost three-fold higher on control HEK cells. The anti-adhesive properties of Endoglycan were explained
207 by its post-translational modification (Supplementary Figure 7). Enzymatic removal of sialic acid by
208 Neuraminidase or of O-linked glycans by O-glycosidase abolished the anti-adhesive properties of Endoglycan
209 expressed in HEK cells.
210 In addition, we tested our hypothesis that Endoglycan was a negative regulator of adhesion by manipulating
211 the balance of adhesion between commissural axons and the floor plate. We had previously used a similar
212 approach to demonstrate a role of RabGDI in Robo trafficking (Philipp et al., 2012). Commissural axons cross
213 the midline because of the positive signals provided by the interaction of floor-plate NrCAM with growth cone
214 Contactin2 (Stoeckli and Landmesser, 1995; Stoeckli et al., 1997; Fitzli et al., 2000). In the absence of NrCAM or
215 Contactin2, commissural axons fail to enter the floor plate and turn into the longitudinal axis prematurely along
216 the ipsilateral floor-plate border. The positive signal derived from the Contactin2/NrCAM interaction depends
217 on sufficient contact between growth cone and floor-plate cells. Thus, we hypothesized that the failure to
218 detect the positive signal due to lower NrCAM levels on the floor-plate cells could be counteracted by a forced
219 increase in growth cone-floor plate contact. We reasoned that the concomitant downregulation of NrCAM and
220 Endoglycan would rescue the NrCAM phenotype, because the decrease in adhesion due to lower NrCAM,
221 resulting in the failure of commissural axons to enter the floor plate, would be counteracted by an increase in
222 adhesion in the absence of Endoglycan. This is indeed what we observed (Figure 5). As found previously
223 (Stoeckli and Landmesser, 1995; Pekarik et al., 2003), axons were frequently turning prematurely along the
224 ipsilateral floor-plate border in the absence of NrCAM (Figure 5A). In accordance with our hypothesis,
225 ipsilateral turns were reduced to control levels when NrCAM and Endoglycan were downregulated
226 concomitantly (Figure 5B,G). The rescue of the NrCAM phenotype was only seen for Endoglycan, as
227 concomitant downregulation of NrCAM with Podocalyxin or CD34 had no effect on ipsilateral turns (Figure 5).
228

229

230 **Endoglycan acts as 'lubricant' for growth cone movement in the floor plate**

231

232 To get more insight into the role of Endoglycan in the regulation of contacts between axons and floor-plate
233 cells, we established ex vivo live imaging of commissural axons during midline crossing. Intact spinal cords of
234 HH22 chicken embryos, which were co-injected and unilaterally electroporated with constructs expressing
235 farnesylated td-Tomato (td-Tomato-f) under the control of the dI1 neuron-specific Math1 enhancer together
236 with farnesylated EGFP (EGFP-f) under the control of the β-actin promoter, were cultured and imaged for 24
237 hours (Figure 6). This method allowed us to follow the behavior and trajectories of the very first wave of single
238 dI1 axons entering, crossing, and exiting the floor plate in a conserved environment (arrowheads, Figure 6A_1-
239 A_3). The expression of EGFP-f in all transfected cells and brightfield images helped us to define the floor-plate
240 boundaries (white dashed lines) and midline (yellow dashed lines in Figure 6B,C).
241 Spinal cords of embryos co-injected with the Math1::tdTomato-f plasmid and dsRNA derived from Endoglycan
242 (dsEndo) or a plasmid encoding chicken Endoglycan under the β-actin promoter (Endo OE) were imaged for 24
243 hours and compared to spinal cords dissected from control-injected embryos (Endo ctrl, Supplementary movie
244 1, temporally color-coded projections in Figure 6D_1,E_1 and F_1). In contrast to control-injected spinal cords, the
245 post-crossing segment of dI1 axons was disorganized in dsEndo and Endo OE conditions. In both these
246 conditions, caudal turns were seen (Supplementary movie 1). As our in vivo data suggested a difference in
247 adhesion between floor-plate cells and dI1 axons, we analyzed axonal midline crossing with kymographs in two
248 different regions of interest (ROI; shown in Figures 6D_1, E_1, F_1). This allowed us to follow growth cone
249 movement across the floor plate and along the floor-plate border. Interestingly, our analyses indicated that the
250 transfection of dsRNA derived from Endoglycan in dI1 neurons and floor-plate cells led to a decrease in the
251 growth cones' speed in the first half of the floor plate (15 µm/h) and in an increase in the second half (51 µm/h;
252 Figure 6E_2) compared to control-injected spinal cords (Figure 6D_2 and Supplementary movie 2), where speed in
253 the first and second halves did not differ (30 µm/h). In spinal cords overexpressing *Endoglycan*, growth cone
254 speed was accelerated in the entire floor plate (59 µm/h; Figure 6F_2; Supplementary movie 2). The analysis of
255 axon growth in a second ROI confirmed the disorganization seen in both mutants in Supplementary movie 1.
256 Whereas the axonal trajectories in control-injected embryos (Figure 6D_3) were well organized and mostly
257 parallel, axonal behavior in mutants caused 'smeared' patterns (asterisks Figure 6E_3) due to stalling and pixels

258 moving obviously in caudal direction indicating caudal axonal turns (arrowheads in Figures $6F_3$). These
259 phenotypes confirmed our analyses of open-book preparations of spinal cords lacking Endoglycan (Figure 1).
260 Axonal stalling (arrowheads) and caudal turns (arrows) could also be observed at the floor-plate exit site of
261 spinal cord overexpressing *Endoglycan* (Supplementary movie 3).
262 The obvious differences in axonal behavior in experimental compared to control spinal cords was corroborated
263 by quantitative analyses of specific aspects. Firstly, we quantified how much time the growth cones spent
264 migrating from the floor-plate entry site to the exit site (Figure $7A_1$). Confirming the observations made in our
265 movies and kymographic analysis, growth cones overexpressing *Endoglycan* crossed the floor plate faster, in
266 only 4.4±1.4 hours (mean±SD), compared to controls (5.4±1.3 hours) and the dsEndo condition (5.5±1.2; Figure
267 7B). Furthermore, we compared the average time for crossing each half of the floor plate for each condition
268 (Figure $7A_1$, C). Growth cones migrated equally fast through both halves in controls (2.7±0.9 hours versus
269 2.6±1.0 hours, Figure 7C). After overexpression of *Endoglycan*, there was a slight but significant shortening of
270 the time growth cones spent crossing the first half compared to the second half (2.1±0.7 hours versus 2.3±0.8
271 hours, Figure 7C). In contrast, the unilateral silencing of *Endoglycan* induced a highly significant difference in
272 the migration speed of growth cones in the first (electroporated) versus the second half of the floor plate. It
273 took 3.1±0.9 hours to cross the first half but only 2.5±1.0 hours to cross the second half (Figure 7C). An
274 alternative way of demonstrating the differences in migration speed is shown in Figure 7D,E. We calculated the
275 ratios of the time spent in the first (Figure 7D) or the second half of the floor plate (Figure 7E) compared to the
276 total time used for floor-plate crossing for the different conditions (Figure 7B). Indeed, knockdown of
277 Endoglycan induced a significant increase in the ratio spent in the first half of the floor plate (0.56±0.1)
278 compared to both control (0.51±0.1) and overexpression of Endoglycan (0.48±0.1; Figure 7D). In the second
279 half of the floor plate, there was a significant decrease in spinal cords electroporated with dsEndo (0.44±0.1)
280 compared to control (0.49±0.1) and *Endoglycan* overexpressing spinal cords (0.52±0.1; Figure 7E).
281 Secondly, we also analyzed growth cone morphologies by comparing the average area in the first and the
282 second halves, as well as at the exit site of the floor plate (Figure $7A_2$). The difference in growth speed was
283 reflected in growth cone morphology and size (Supplementary Figure 8 and Supplementary movie 1). Growth
284 cones tended to be small and have a simple morphology at fast speed. At choice points, like the floor-plate exit
285 site, growth cone size and complexity increased. The average area of growth cones in the floor plate in control
286 spinal cords was 68±18 μm^2 in the first, and 65±16 μm^2 in the second half of the floor plate (Supplementary

287 Figure 8A). The growth cone area significantly increased at the floor-plate exit site, where growth cones need
288 to choose to grow rostrally rather than caudally (Supplementary Figure 8A). At the exit site, growth cone area
289 was 145±39 μm^2 in control embryos. In agreement with their faster speed in the floor plate overexpressing
290 *Endoglycan*, growth cones were significantly smaller in the first (60±20 μm^2) and the second half (56±14 μm^2)
291 of the floor plate, as well as at the exit site (120±38 μm^2) compared to controls (Figure 7F-H and Supplementary
292 Figure 8C). Reduction of Endoglycan expression in the axons and in the first half of the floor plate resulted in
293 reduced migration speed, but the average size of the growth cones was not significantly different from
294 controls. (Figure 7F). The fact that growth cone were significantly faster in the second, non-transfected half of
295 the floor plate was reflected by a significant reduction in growth cone area (56±14 μm^2) compared to control
296 (68±18 μm^2) and compared to the first, transfected half (67±18 μm^2; Figure 7G, Supplementary Figure 8B, Table
297 2).
298
299 Finally, live imaging of growth cones crossing the floor plate provided support for our hypothesis that axon-
300 floor plate contact was causing the displacement of floor-plate cells observed after knockdown of *Endoglycan*,
301 the 'corkscrew' phenotype. The tortuous, corkscrew-like phenotype of axons was seen exclusively in spinal
302 cords after knockdown of *Endoglycan* (Figure 8 and Supplementary movies 4 and 5). We could observe
303 roundish EGFP-f-positive cells (arrows) that obstructed the smooth trajectory of dI1 axons in the commissure
304 (arrowheads in Figure $8A_{1-5}$ and Supplementary movie 4). Although we could not use markers to identify these
305 cells as floor-plate cells, their position indicated that they had to be mislocalized floor-plate cells. Moreover,
306 dI1 axons were found to form loops in the layer where floor-plate cell somata were localized (arrowhead in
307 Figure $8B_{1-5}$ and Supplementary movie 5). In the first half of the floor plate electroporated with dsEndo, clusters
308 of roundish EGFP-f-positive cells in the commissure (arrows) were apparently causing axons to deviate from
309 their trajectory by strongly adhering to them (arrowheads in Figure $8C_{1-5}$ and Supplementary movie 5). We
310 never found such aberrant behavior in control embryos or in embryos overexpressing *Endoglycan*. Moreover,
311 we only observed these events after many dI1 axons had already crossed the floor plate (after at least 10
312 hours), supporting the hypothesis that the phenotype was due to excessive growth cone-floor plate adhesion
313 resulting in floor-plate cell displacement. Furthermore, these observations suggest that Endoglycan regulates
314 migratory speed of growth cones by modulating their adhesion to floor-plate cells.

Taken together, our live imaging studies support results from in vitro adhesion experiments indicating that the level of Endoglycan expression modulates adhesive strength between dI1 commissural growth cones and floor-plate cells. In contrast, axon-axon interactions did not seem to be different in the presence and absence of Endoglycan, as we did not find any effect on pre-crossing axons after perturbation of Endoglycan levels (Supplementary Figure 9).

Endoglycan is expressed in migrating Purkinje cells and is required for their radial migration

In the developing cerebellum, *Endoglycan* expression was found exclusively in migrating Purkinje cells (Figure 9). Purkinje cells are born in the ventricular zone of the cerebellar anlage (Hatten, 1999). From there, they migrate radially toward the periphery to form the distinct Purkinje cell layer (Figure 9A-F). At HH44, when Purkinje cells migration is completed, *Endoglycan* mRNA is no longer detectable in Purkinje cells (Figure 9F). To test our hypothesis that Endoglycan was required as a 'lubricant' or regulator of cell-cell adhesion in a different situation, we analyzed the migratory behavior of Purkinje cells. To this end, we injected and electroporated dsRNA derived from *Endoglycan* into the developing cerebellum at HH34. Control embryos were injected and transfected only with a plasmid encoding EGFP (Figure 10). In untreated control embryos at HH38, the Purkinje cell layer is still more than one cell diameter in width but is clearly detectable in the periphery of the cerebellar lobes (Figure 10B,C). Very few, if any, Purkinje cells were found in the center of the lobes. The same was true in embryos injected with the EGFP-expression plasmid only (Figure 10D-F). In contrast, Purkinje cells were still found in the center of the lobes and close to the ventricular zone in HH38 embryos treated with dsRNA derived from *Endoglycan* (Figure 10G-I,J,M). In addition, the gross morphology of the cerebellum was severely compromised, because individual lobes failed to separate. Overall the size of the cerebellum was significantly reduced (Figure 10K,L,N,O).

Aberrant migration of Purkinje cells reduces granule cell proliferation

Purkinje cells regulate the proliferation of granule cells by releasing Shh (Sonic hedgehog), which stimulates proliferation of granule cell precursors in the outer EGL (external granule cell layer) (Dahmane and Ruiz i

Altaba, 1999; Wechsler-Reya and Scott, 1999; Wallace, 1999; Lewis et al., 2004; reviewed in De Luca et al., 2016). In turn, reduced proliferation of granule cells was shown to result in changes of cerebellar morphology similar to the ones we observed after downregulation of Endoglycan (Figure 10) (Lewis et al., 2004). A reduced rate of granule cell proliferation was indeed what we found in embryos after silencing *Endoglycan*. When we used Pax6 as a marker for granule cells, we found a thinner EGL in experimental embryos compared to control-treated and untreated embryos (Figure 11A-D). This decrease in EGL width was due to a reduced proliferation rate of granule cells rather than apoptosis (Figure 11E-H). In contrast to granule cells, the proliferation rate of Purkinje cells and other cells born in the ventricular zone at HH35 did not differ between control embryos and embryos lacking Endoglycan (Figure 11I-K).

In summary, our results demonstrate a vital role for Endoglycan in commissural axon guidance at the ventral midline and Purkinje cell migration in the developing cerebellum. In both systems, the observed phenotype is consistent with the hypothesis that Endoglycan is an essential regulator of cell-cell contacts by modulating the strength of adhesion between cells. This model is supported by observations in vitro and in vivo. Neuronal attachment was negatively affected by the presence of an excess of Endoglycan in a glycosylation-dependent manner, indicating that Endoglycan decreases adhesive strength during neural circuit assembly.

DISCUSSION

We identified *Endoglycan*, a member of the CD34 family of sialomucins, in a screen for axon guidance cues involved in commissural axon pathfinding at the midline of the spinal cord. In the developing chicken cerebellum, *Endoglycan* is expressed exclusively in Purkinje cells during their migration from the ventricular zone to their final destination in the periphery of the cerebellar lobes (Figure 9). In the absence of Endoglycan, Purkinje cells failed to migrate and accumulated in the center of the cerebellar folds (Figure 10). This observation suggests a role of Endoglycan as 'lubricant' that is supported by the structural features of sialomucins. The function of CD34 family members has not been characterized in detail but all the results

373 obtained so far are compatible with an anti-adhesive role (Nielsen and McNagny, 2008). One exception are
374 reports from the lymph node cells, the so-called high endothelial venules (HEVs) where a very specific
375 glycosylation patterns was implicated in the interaction of CD34 and Endoglycan with L-selectin (Furness and
376 McNagny, 2006). However, in agreement with most published studies on the role of CD34 and Podocalyxin (for
377 reviews see Furness and McNagny, 2006; Nielsen and McNagny, 2008 and 2009) our observations suggest that
378 Endoglycan acts as a 'lubricant' rather than as adhesive factor. This model is supported by results from in vivo
379 and in vitro experiments that confirm a negative effect of Endoglycan on cell-cell adhesion (Figure 12).
380 The adhesion-modulating effect of Endoglycan is mediated by the negatively charged mucin domain. Similar to
381 the role suggested for the polysialic acid modification of NCAM (Rutishauser, 2008; Brusés and Rutishauser,
382 2001; Burgess et al., 2008), Endoglycan could lower cell-cell adhesion by increasing the distance between
383 adjacent cell membranes due to repulsion caused by the bulky, negatively charged posttranslational
384 modifications of its extracellular domains. A similar effect was found for PSA-NCAM in hindlimb innervation
385 (Tang et al., 1994; Landmesser et al., 1990) and in the visual system, where retinal ganglion cell axons
386 innervating the tectum were found to regulate axon-axon adhesion versus axon-target cell adhesion
387 (Rutishauser et al., 1988). The same mechanism was found in motoneurons, where axon-axon versus axon-
388 muscle fiber adhesion was a determining factor for the appropriate innervation pattern. In contrast to PSA-
389 NCAM that continues to play a role in synaptic plasticity in the adult nervous system, the function of
390 Endoglycan appears to be restricted to development. Expression of *Endoglycan* ceased in the cerebellum after
391 the mature wiring pattern was achieved.
392
393 At first sight, the effect of Endoglycan on floor-plate morphology appears to suggest a positive regulation of
394 cell-cell adhesion. Floor-plate cells are precisely aligned in control embryos but are protruding into the
395 commissure in the absence of Endoglycan. Therefore, one might conclude that in the absence of Endoglycan
396 cell-cell adhesion between floor-plate cells is compromised, resulting in the observed structural changes.
397 However, this scenario can be ruled out based on the analysis of younger embryos. At HH21, the floor plate
398 was intact in the absence of Endoglycan, indicating that Endoglycan is not required for adhesion between floor-
399 plate cells. The morphology of the floor plate is only compromised once many axons have crossed the midline.
400 These findings are supported by our live imaging data of growth cones crossing the floor plate. Contacts
401 between commissural axons and floor-plate cells have to be broken when later crossing commissural axons

402 arrive and cross (Yaginuma et al., 1991). Commissural axons crossing the floor plate are suggested to do so by
403 close interaction with short filopodial processes of floor-plate cells. Thus, the aberrant morphology of the floor
404 plate at HH25 is explained by the inability of axons to break contacts with floor-plate cells in the absence of
405 Endoglycan, consistent with our hypothesis that Endoglycan is a negative regulator of adhesion by acting as a
406 'lubricant'. Live imaging data demonstrated that the perturbation of the balance in growth cone-floor plate
407 adhesion led to impaired timing of midline crossing, which in turn might also interfere with the correct sensing
408 and reading of guidance cues by dI1 growth cones, and prevented them from making the correct decision at
409 the floor-plate exit site.
410
411 Thus, we concluded that the function of Endoglycan in commissural axon guidance and in Purkinje cell
412 migration is to lower cell adhesion. In both cases, the absence of Endoglycan results in too much stickiness. In
413 the cerebellum, excessive adhesion prevents the Purkinje cells from migrating to their target layer. At the
414 midline of the spinal cord, excessive adhesion causes axons to adhere too much to floor-plate cells and
415 prevents their displacement by follower axons. Rather than acting as a guidance cue or guidance receptor, we
416 suggest that Endoglycan affects neural circuit formation by modulating the interaction of many different
417 guidance cues and their surface receptors.
418
419 In summary, we propose an 'anti-adhesive' role for Endoglycan in axon guidance and neural migration that is
420 fine-tuning the balance between adhesion and de-adhesion (Figure 12). Precise regulation of cell-cell contacts
421 is required in both processes and is fundamental for developmental processes that depend on a high degree of
422 plasticity and a plethora of specific molecular interactions.
423
424
425
426 **METHODS**
427
428 **Identification and Cloning of *Endoglycan***
429 We had used a PCR-based subtractive hybridization screen to search for guidance cues for post-crossing
430 commissural axons (for details, see Bourikas et al., 2005). To this end, we isolated floor-plate cells from HH26

431 and HH20 embryos (Hamburger and Hamilton, 1951). Among the differentially expressed genes, we found a
432 sequence from the 3'-UTR of *Endoglycan*. Subsequently, a cDNA fragment from the coding sequence of
433 *Endoglycan* (PODXL2; 1028-1546 bp) was obtained by RT-PCR using total RNA isolated from HH40 cerebellum.
434 For reverse transcription, 1 µg total RNA was mixed with 0.3 µl RNasin (Promega), 1 µl dNTPs (5 mM), 1 µl
435 random nonamers, 1 µl DTT (Promega), in 20 µl Superscript II buffer (Invitrogen). Reverse transcription was
436 carried out for 1 hour at 42°C. Two µl of this mixture were used for PCR with 2.5 µl forward primer (10 µM; 5'-
437 CAGACACGCAGACTCTTTC-3') and 2.5 µl reverse primer (10 µM; 5'-CTAAAGATGTGTGTCTTCCTCA-3') using the
438 Expand Long Template PCR System (Roche). The PCR conditions were 35 cycles at 95°C for 30 sec, 57°C for 30
439 sec and 68°C for 3 min. The PCR product was cut with BamHI/BclI and cloned into pBluescript II KS. For cloning
440 of full-length chicken Endoglycan, we used 5'-ATGGTGAGAGGAGCTGCG-3' and 5'-
441 GTGTTTGAGGAAGACACACATCTTTAG-3' as forward and reverse primers, respectively. A plasmid containing the
442 full-length ORF of human *Endoglycan* was obtained from SourceBiosource.
443
444 **Preparation of DIG-labeled RNA probes and in situ hybridization**
445 For in vitro transcription, 1 µg of the linearized and purified plasmids encoding Endoglycan (EndoORF: 1028-
446 1546pb, Endo3'UTR: 3150-3743bp and 5070-5754bp; numbers are derived from the human sequence),
447 Podocalyxin (ChEST190L9) and CD34 (ChEST91D7) were used to prepare DIG-labeled in situ probes as described
448 earlier (Mauti et al., 2006). The same fragments were used to prepare dsRNA (Pekarik et al., 2003; Baeriswyl et
449 al., 2008; Andermatt and Stoeckli, 2014b).
450
451 **Northern Blot**
452 Total RNA was extracted from cerebrum, cerebellum, spinal cord, muscle, heart, lung and kidney from HH38
453 embryos using the RNeasy Mini Kit (Qiagen) and loaded on a denaturing formaldehyde gel (4.5 µg of total RNA
454 per lane). The RNA was blotted onto a positively charged nylon membrane (Roche) overnight using 10x SSC as a
455 transfer medium. The membranes were hybridized with 1.5 µg preheated DIG-labeled RNA probes for
456 *Endoglycan* and *GAPDH* at 68°C overnight. The membrane was then washed twice with 2xSSC/0.1%SDS for 5
457 minutes at room temperature and twice with 0.1xSSC/0.5% SDS for 20 minutes at 68°C. For detection, buffer 2
458 (2% blocking reagent dissolved in 0.1 M maleic acid, 0.15 M NaCl, pH 7.5) was added for 2-3 hours at room
459 temperature. After incubation with anti-digoxigenin-AP antibody dissolved in buffer 2 (1:10,000; Roche) for 30

460 minutes at room temperature the membrane was washed twice in washing buffer (0.3% Tween 20 dissolved in
461 0.1 M maleic acid, 0.15 M NaCl, pH 7.5) for 20 minutes. Subsequently, detection buffer (0.1 M Tris-HCl, 0.1 M
462 NaCl, pH 9.5) was applied for 2 minutes before adding CDP-star (25 mM, Roche) for 5 minutes in the dark. For
463 detection of the chemiluminescence a Kodak BioMAX XAR film was used.
464
465 **In ovo RNAi**
466 For functional studies in the spinal cord, we silenced *Endoglycan* with three different long dsRNAs. They were
467 produced from bp 1028-1546 of the ORF, as well as bp 3150-3743 and bp 5070-5754 from the 3'UTR. The fact
468 that we obtained the same phenotype with three different, non-overlapping dsRNAs derived from *Endoglycan*
469 confirms the specificity of the approach and the absence of off-target effects. dsRNA was produced as detailed
470 in Pekarik et al., 2003 and Wilson and Stoeckli, 2011. Because no antibodies recognizing chicken Endoglycan are
471 available, we used in situ hybridization to assess the successful downregulation of the target mRNA
472 (Supplementary Figure 10). Downregulation efficiency was about 40%. Because we transfect only around 50%
473 of the cells in the electroporated area, transfected cells express only very low levels of Endoglycan.
474 For rescue experiments, the dsRNA was co-injected with 150 (low), 300 (middle), or 750 ng/µl (high) plasmid
475 encoding the ORF of chicken *Endoglycan*. The ORF was either expressed under the control of the Math1
476 promoter for dI1 neuron-specific expression, or the Hoxa1 promoter for floor-plate specific expression of
477 *Endoglycan*.
478
479 **Ex ovo RNAi**
480 To analyze the in vivo function of Endoglycan in the developing cerebellum, ex ovo cultures of chicken embryos
481 were prepared (Baeriswyl and Stoeckli, 2008; Andermatt and Stoeckli, 2014b). Injections and electroporations
482 were performed at E8 (HH34). To have direct access to the embryo a small hole of 3 to 4 mm diameter was cut
483 into the extraembryonic membranes above the eye. For positioning and stabilization of the head during
484 injection and subsequent electroporation, we used a hook prepared from a spatula. Approximately 1 µl of the
485 nucleic acid mixture, consisting of a plasmid encoding EGFP under the control of the β-actin promoter (100
486 ng/µl), dsRNA derived from the ORF of *Endoglycan* (500 ng/µl), and 0.04% (vol/vol) Trypan Blue (Invitrogen)
487 dissolved in sterile PBS was injected into the cerebellum, using a borosilicate glass capillary with a tip diameter
488 of 5 µm (World Precision Instruments). Before electroporation, a few drops of sterile PBS were added to the

489 embryo. For the electroporation, a platelet electrode of 7 mm diameter (Tweezertrodes Model #520, BTX
490 Instrument Division, Harvard Apparatus) was placed collaterally to the head of the embryo. Six pulses of 40 V
491 and 99 ms duration were applied using a square wave electroporator (ECM830, BTX).
492
493 **Motoneuron adhesion assay**
494 Dissociated motoneurons of HH26 chicken embryos were cultured as described previously (Mauti et al., 2006)
495 either on HEK293T cells stably expressing human Endoglycan-myc under the control of the CMV promoter or
496 on untransfected HEK293T cells as control. The plasmid encoding human Endoglycan was obtained from
497 SourceBioScience (Nottingham, UK). After 40h, the cultures were fixed for 1h at room temperature in 4%
498 paraformaldehyde and stained with mouse anti-neurofilament (RMO 270; Zymed) and rabbit anti-myc
499 antibodies (Abcam). The number of neurofilament-positive cells was counted in 16 randomly selected frames
500 (0.4 mm^2). Similar results were obtained in 3 independent experiments. One representative example is shown
501 in Figure 4. In a separate set of experiments, cultured HEK cells expressing Endoglycan were treated with O-
502 glycosidase (8'000 U/ml; NEB) or α2-3,6,8 Neuraminidase (5 U/ml; NEB) for 2 hours before motoneurons were
503 added (Supplementary Figure 7).
504
505 **Tissue preparation and analysis**
506 To analyze commissural axon growth and guidance the embryos were sacrificed between HH25 and 26. The
507 spinal cord was removed, opened at the roof plate ('open-book' preparation) and fixed in 4%
508 paraformaldehyde (PFA) for 40 min to 1 hour at room temperature. To visualize the trajectories of commissural
509 axons, Fast-Dil (5 mg/ml, dissolved in ethanol, Molecular Probes) was injected into the dorsal part of the spinal
510 cord as described previously (Wilson and Stoeckli, 2012). For the analysis of the cerebellum, the embryos were
511 sacrificed one to four days after electroporation. The whole brain was removed and analyzed for EGFP
512 expression using a fluorescence stereomicroscope (Olympus SZX12). The brain tissue was fixed for two hours at
513 room temperature in 4% PFA in PBS. After fixation, the brain tissue was rinsed in PBS and transferred to 25%
514 sucrose in 0.1M sodium phosphate buffer, pH 7.4, for cryoprotection. In this study, 30 µm-thick sagittal
515 cryostat sections were used for analysis. For the preparation of cryostat sections, the brains were embedded in
516 O.C.T Tissue-Tek (Sakura) in Peel-a-Way® disposable embedding molds (Polysciences), frozen in isopentane on

517 dry ice and cut on a cryocut (CM1850, Leica Microsystems). The sections were collected on SuperFrost®Plus
518 microscope slides (Menzel-Glaeser).
519
520 **Immunohistochemistry**
521 Cryostat sections were rinsed in PBS at 37°C for 3 minutes followed by 3 minutes in cold water. Subsequently
522 the sections were incubated in 20 mM lysine in 0.1 M sodium phosphate (pH 7.4) for 30 minutes at room
523 temperature before being rinsed in PBS three times for 10 minutes. The tissue was permeabilized with 0.1%
524 Triton in PBS for 30 minutes at room temperature and then washed again three times with PBS for 10 minutes.
525 To prevent unspecific binding of the antibody the tissue was blocked with 10% fetal calf serum (FCS) in PBS for
526 one hour. Rabbit anti-GFP (1:250; Abcam), anti-axonin-1 (rabbit 1:1000 or goat 1:500), anti-NrCAM (goat
527 1:1000), anti-Calbindin D-28K (1:2000, CB38a; Swant), mouse anti-HNF3β (supernatant; 4C7, DSHB), mouse
528 anti-Islet1 (supernatant; 40.2D6, DSHB), mouse anti-Nkx2.2 (supernatant; 74.5A5, DSHB), mouse anti-Pax3 and
529 Pax6 (supernatant, DSHB) were dissolved in 10% FCS/PBS and incubated overnight at 4°C. After three washes in
530 PBS, 10% FCS in PBS was applied again for one hour, followed by the incubation with goat anti-rabbit IgG-
531 Alexa488 (1:250; Molecular Probes), donkey anti-rabbit IgG-Cy3 (1:200; Jackson ImmunoResearch) or goat anti-
532 mouse IgG-Cy3 (1:250; Jackson ImmunoResearch) diluted in 10% FCS in PBS for 90 minutes at room
533 temperature. The tissue was rinsed 5 times in PBS for 12 minutes and then mounted in Celvol (Celanese) or
534 Mowiol. The staining of cryostat sections was analyzed with an upright microscope equipped with fluorescence
535 optics (Olympus BX51).
536
537 **Analysis of cell proliferation and cell death**
538 To assess cell proliferation in the developing cerebellum, we used BrdU incorporation. Embryos were injected
539 and electroporated at HH34 with dsRNA derived from *Endoglycan* and the *EGFP* plasmid or with the *EGFP*
540 plasmid alone. After 1 (HH35) or 4 days (HH38), 200 µl 50 mM BrdU in H_2O were pipetted onto the
541 chorioallantois. After 3 h the embryos were sacrificed, the brains were dissected and prepared for cryostat
542 sections as described above. For visualization of the incorporated BrdU, the sections were incubated in 50%
543 formamide in 2xSSC for 1 to 2 h at 65 °C, rinsed twice in 2xSSC for 15 min followed by incubation in 2 N HCl for
544 30 min at 37 °C. Sections were rinsed in 0.1 M borate buffer (pH 8.5) for 10 min at room temperature, followed

545 by PBS (six changes). BrdU was detected with mouse anti-BrdU (Sigma; 1:200) using the protocol detailed
546 above. Sections were counterstained with DAPI (5 µg/ml in PBS) for 20 min at room temperature.
547 Apoptosis was analyzed as described previously (Baeriswyl and Stoeckli, 2008). For analysis of cell death in the
548 floor plate, we used cleaved caspase-3 staining of sections taken from HH25 embryos.
549
550 **Quantification**
551 DiI injections sites with pathfinding errors were analyzed and counted, using an upright microscope equipped
552 with fluorescence optics (Olympus BX51). All measurements including floor-plate width, thickness of the
553 commissure, spinal cord width, Calbindin fluorescence intensities, real and outer cerebellar circumference, EGL
554 thickness, and number of BrdU positive cells were performed with the analySIS Five software from Soft Imaging
555 System. For all measurements, embryos injected with dsRNA derived from *Endoglycan* were compared with
556 embryos injected with the EGFP plasmid only, and untreated controls. For statistical analyses, ANOVA with
557 Bonferroni correction was used except for the rescue experiments, where Tukey's multiple comparison test
558 was used instead. Values are given as mean ± SEM. *: $P < 0.05$. **: $P < 0.01$. ***: $P < 0.001$.
559
560 **Live imaging**
561 Plasmids encoding farnesylated td-Tomato under the Math1 enhancer upstream of the β-globin minimal
562 promoter for dI1 neuron-specific expression (Math1::tdTomato-f) and farnesylated EGFP under the β-actin
563 promoter (β-actin::EGFP-f) were co-injected into the central canal of the chicken neural tube in ovo at HH17/18
564 and unilaterally electroporated, using a BTX ECM830 square-wave electroporator (five pulses at 25 V with 50
565 ms duration each), as previously described (Wilson and Stoeckli, 2012). For the perturbation of Endoglycan
566 levels, either 300 ng/µl dsRNA derived from the 3'-UTR of Endoglycan or a plasmid encoding the open-reading
567 frame of Endoglycan under the β-actin promoter were co-injected with the Math1::tdTomato-f plasmid. After
568 electroporation, embryos were covered with sterile PBS and eggs were sealed with tape and incubated at 39°C
569 for 26-30 hours until embryos reached stage HH22.
570 For live imaging, embryos were sacrificed at HH22. Intact spinal cords were dissected and embedded with the
571 ventral side down in a drop (100 µl) of 0.5% low-melting agarose (FMC; Pignata et al., 2019) containing a 6:7
572 ratio of spinal cord medium (MEM with Glutamax (Gibco) supplemented with 4 mg/ml Albumax (Gibco), 1 mM
573 pyruvate (Sigma), 100 Units/ml Penicillin and 100 µg/ml Streptomycin in a 35-mm Ibidi µ-Dish with glass

574 bottom (Ibidi, #81158). Once the agarose polymerized, 200 µl of spinal cord medium were added to the drop
575 and live imaging was started.
576 Live imaging recordings were carried out with an Olympus IX83 inverted microscope equipped with a spinning
577 disk unit (CSU-X1 10'000 rpm, Yokogawa). Cultured spinal cords were kept at 37°C with 5% CO_2 and 95% air in a
578 PeCon cell vivo chamber. Temperature and CO_2-levels were controlled by the cell vivo temperature controller
579 and the CO_2 controller units (PeCon). Spinal cords were incubated for at least 30 min before imaging was
580 started. We acquired 18-35 planes (1.5 µm spacing) of 2x2 binned z-stack images every 15 min for 24 hours
581 with a 20x air objective (UPLSAPO 20x/0.75, Olympus) and an Orca-Flash 4.0 camera (Hamamatsu) with the
582 help of Olympus CellSens Dimension 2.2 software. Z-stacks and maximum projections of Z-stack movies were
583 evaluated and processed using Fiji/ImageJ (Schindelin et al., 2012). Temporally color-coded projections were
584 generated using Fiji/ImageJ. Kymograph analysis of axons crossing the floor plate or exiting it was performed as
585 previously described (Medioni et al., 2015) using a region of interest (ROI) selection, the re-slice function and
586 the z-projection of the re-sliced results in Fiji/ImageJ, which allowed following pixel movements within the
587 horizontal axis. The ROI in the floor plate was selected as a 120x20 μm^2 rectangle and the one in the post-
588 crossing segment was a rectangle of 175x104 μm^2. Note that the post-crossing segment ROI was rotated by 90°
589 before running the kymograph analysis. The MtrackJ plugin (Meijering et al., 2012) was used to virtually trace
590 single tdTomato-positive dI1 axons crossing the floor plate. Only axons that enter, cross and exit the floor plate
591 during the 24-hour imaging period were traced and quantified. Overlays of traced axons with GFP and
592 brightfield channels were used to assess the time the axons needed to cross the floor plate. Videos of axons
593 with the 'corkscrew' phenotype were generated and assembled from z-stacks that were 2D deconvolved
594 (nearest neighbor) using the Olympus CellSens Dimension 2.2 and Fiji/Image J software, respectively.
595
596
597
598 **Acknowledgements**
599 We thank Dr. Beat Kunz and Tiziana Flego for excellent technical assistance, Alexandra Moniz and John Darby
600 Cole for help with glycosylation dependence experiment, and members of the lab for discussions and critical
601 reading of the manuscript. This project was supported by the Swiss National Science Foundation and the NCCR
602 Brain Plasticity and Repair (Center of Transgenesis Expertise).

603

604 **References**

605

606 Andermatt, I., Wilson, N.H., Bergmann, T., Mauti, O., Gesemann, M., Sockanathan, S., and Stoeckli, E.T. (2014a).
607 Semaphorin 6B acts as a receptor in post-crossing commissural axon guidance. Development *141*, 3709–3720.

608 Andermatt, I., and Stoeckli, E.T. (2014b). RNAi-based gene silencing in chicken brain development. Methods
609 Mol. Biol *1082*, 253–266.

610 Augsburger, A., Schuchardt, A., Hoskins, S., Dodd, J., and Butler, S. (1999). BMPs as mediators of roof plate
611 repulsion of commissural neurons. Neuron *24*, 127–141.

612 Avilés, E.C., and Stoeckli, E.T. (2016). Canonical wnt signaling is required for commissural axon guidance. Dev.
613 Neurobiol. *76*, 190–208.

614 Baeriswyl, T., and Stoeckli, E.T. (2008). Axonin-1/TAG-1 is required for pathfinding of granule cell axons in the
615 developing cerebellum. Neural Dev. *3*, 7.

616 Baeriswyl, T., Mauti, O., and Stoeckli, E.T. (2008). Temporal control of gene silencing by in ovo electroporation.
617 Methods Mol. Biol. *442*, 231–244.

618 Blockus, H., and Chédotal, A. (2016). Slit-Robo signaling. Development *143*, 3037–3044.

619 Bourikas, D., Pekarik, V., Baeriswyl, T., Grunditz, A., Sadhu, R., Nardó, M., and Stoeckli, E.T. (2005). Sonic
620 hedgehog guides commissural axons along the longitudinal axis of the spinal cord. Nature Neurosci. *8*, 297–
621 304.

622 Boyer, N.P., and Gupton, S.L. (2018). Revisiting Netrin-1. One Who Guides (Axons). Frontiers Cell. Neurosci. *12*,
623 221.

624 Brusés, J.L., and Rutishauser, U. (2001). Roles, regulation, and mechanism of polysialic acid function during
625 neural development. Biochimie *83*, 635–643.

626 Burgess, A., Wainwright, S.R., Shihabuddin, L.S., Rutishauser, U., Seki, T., and Aubert, I. (2008). Polysialic acid
627 regulates the clustering, migration, and neuronal differentiation of progenitor cells in the adult hippocampus.
628 Dev. Neurobiol. *68*, 1580–1590.

629 Charoy, C., Nawabi, H., Reynaud, F., Derrington, E., Bozon, M., Wright, K., Falk, J., Helmbacher, F., Kindbeiter,
630 K., and Castellani, V. (2012). gdnf activates midline repulsion by Semaphorin3B via NCAM during commissural
631 axon guidance. Neuron *75*, 1051–1066.

632 Dahmane, N., and Ruiz i Altaba, A. (1999). Sonic hedgehog regulates the growth and patterning of the
633 cerebellum. Development *126*, 3089–3100.

634 De Luca, A., Cerrato, V. Fucà, E., Parmigiani, E., Buffo, A., and Leto, K. (2016). Sonic hedgehog patterning during
635 cerebellar development. Cell Mol. Life Sci. *73*, 291-303.

636 De Ramon Francàs, G., Zuñiga, N.R., and Stoeckli, E.T. (2017). The spinal cord shows the way - How axons
637 navigate intermediate targets. Dev. Biol. *432*, 43–52.

638 Domanitskaya, E., Wacker, A., Mauti, O., Baeriswyl, T., Esteve, P., Bovolenta, P., and Stoeckli, E.T. (2010). Sonic
639 hedgehog guides post-crossing commissural axons both directly and indirectly by regulating Wnt activity. J.
640 Neurosci. *30*, 11167–11176.

641 Doyonnas, R., Kershaw, D.B., Duhme, C., Merkens, H., Chelliah, S., Graf, T., and McNagny, K.M. (2001). Anuria,
642 omphalocele, and perinatal lethality in mice lacking the CD34-related protein podocalyxin. J. Exp. Med. *194*,
643 13–27.

644 Doyonnas, R., Nielsen, J.S., Chelliah, S., Drew, E., Hara, T., Miyajima, A., and McNagny, K.M. (2005). Podocalyxin
645 is a CD34-related marker of murine hematopoietic stem cells and embryonic erythroid cells. Blood *105*, 4170–
646 4178.

647 Edgar RC. MUSCLE: a multiple sequence alignment method with reduced time and space complexity. BMC
648 Bioinformatics. 5:113. PubMed PMID: 15318951

649 Fitzli, D., Stoeckli, E.T., Kunz, S., Siribour, K., Rader, C., Kunz, B., Kozlov, S.V., Buchstaller, A., Lane, R.P., Suter,
650 D.M., Dreyer, W.J., and Sonderegger, P. (2000). A Direct Interaction of Axonin-1 with Ngcam-Related Cell
651 Adhesion Molecule (Nrcam) Results in Guidance, but Not Growth of Commissural Axons. J. Cell Biol. *149*, 951–
652 968.

653 Furness, S.G.B., and McNagny, K. (2006). Beyond mere markers. Functions for CD34 family of sialomucins in
654 hematopoiesis. Immunol. Res. *34*, 13–32.

655 Gomez, T.M., and Letourneau, P.C. (2014). Actin dynamics in growth cone motility and navigation. J.
656 Neurochem. *129*, 221–234.

657 Hamburger, V., and Hamilton, H.L. (1951). A series of normal stages in the development of the chick embryo. J.
658 Morphol. *88*, 49–92.

659 Hatten, M.E. (1999). Central nervous system neuronal migration. Annu. Rev. Neurosci. *22*, 511–539.

660 Islam, S.M., Shinmyo, Y., Okafuji, T., Su, Y., Naser, I.B., Ahmed, G., Zhang, S., Chen, S., Ohta, K., Kiyonari, H., Abe,
661 T., Tanaka, S., Nishinakamura, R., Terashima, T., Kitamura, T., and Tanaka, H. (2009). Draxin, a repulsive
662 guidance protein for spinal cord and forebrain commissures. Science *323*, 388–393.

663 Kerjaschki, D., Sharkey, D.J., and Farquhar, M.G. (1984). Identification and characterization of podocalyxin--the
664 major sialoprotein of the renal glomerular epithelial cell. J. Cell Biol. *98*, 1591–1596.

Landmesser, L., Dahm, L., Tang, J.C., and Rutishauser, U. (1990). Polysialic acid as a regulator of intramuscular nerve branching during embryonic development. Neuron *4*, 655–667.

Lewis, P.M., Gritli-Linde, A., Smeyne, R., Kottmann, A., and McMahon, A.P. (2004). Sonic hedgehog signaling is required for expansion of granule neuron precursors and patterning of the mouse cerebellum. Dev. Biol. *270*, 393–410.

Long, H., Sabatier, C., Le Ma, Plump, A., Yuan, W., Ornitz, D.M., Tamada, A., Murakami, F., Goodman, C.S., and Tessier-Lavigne, M. (2004). Conserved roles for Slit and Robo proteins in midline commissural axon guidance. Neuron *42*, 213–223.

Lyuksyutova, A.I., Lu, C.-C., Milanesio, N., King, L.A., Guo, N., Wang, Y., Nathans, J., Tessier-Lavigne, M., and Zou, Y. (2003). Anterior-posterior guidance of commissural axons by Wnt-frizzled signaling. Science *302*, 1984–1988.

Mauti, O., Sadhu, R., Gemayel, J., Gesemann, M., and Stoeckli, E.T. (2006). Expression patterns of plexins and neuropilins are consistent with cooperative and separate functions during neural development. BMC Dev. Biol. *6*, 32.

Medioni, C., Ephrussi, A. and Besse, F. (2015). Live imaging of axonal transport in Drosophila pupal brain explants. Nature Prot. *10*, 574–584.

Meijering, E., Dzyubachyk, O., Smal, I. (2012). Methods for Cell and Particle Tracking. Methods Enzymol. *504*, 183-200.

Nawabi, H., Briançon-Marjollet, A., Clark, C., Sanyas, I., Takamatsu, H., Okuno, T., Kumanogoh, A., Bozon, M., Takeshima, K., Yoshida, Y., Moret, F., Abouzid, K., and Castellani, V. (2010). A midline switch of receptor processing regulates commissural axon guidance in vertebrates. Genes & Dev. *24*, 396–410.

Nielsen, J.S., Graves, M.L., Chelliah, S., Vogl, A.W., Roskelley, C.D., and McNagny, K.M. (2007). The CD34-related molecule podocalyxin is a potent inducer of microvillus formation. PloS one *2*, e237.

Nielsen, J.S., and McNagny, K.M. (2008). Novel functions of the CD34 family. J. Cell Sci. *121*, 3683–3692.

Nielsen, J.S., and McNagny, K.M. (2009). The role of podocalyxin in health and disease. J. Am. Soc. Nephrol. *20*, 1669–1676.

Parra, L.M., and Zou, Y. (2010). Sonic hedgehog induces response of commissural axons to Semaphorin repulsion during midline crossing. Nature Neurosci. *13*, 29–35.

Pekarik, V., Bourikas, D., Miglino, N., Joset, P., Preiswerk, S., and Stoeckli, E.T. (2003). Screening for gene function in chicken embryo using RNAi and electroporation. Nature Biotechnol. *21*, 93–96.

695 Philipp, M., Niederkofler, V., Debrunner, M., Alther, T., Kunz, B., and Stoeckli, E.T. (2012). RabGDI controls
696 axonal midline crossing by regulating Robo1 surface expression. Neural Dev. *7*, 36.

697 Pignata, A., Ducuing, H., Boubakar, L., Gardette, T., Kindbeiter, K., Bozon, M., Tauszig-Delamasure, S., Falk, J.,
698 Thoumine, O. and Castellani, V. (2019). A Spatiotemporal Sequence of Sensitization to Slits and Semaphorins
699 Orchestrates Commissural Axon Navigation. Cell Rep. *29*, 347-362.e5.

700 Ruiz de Almodovar, C., Fabre, P.J., Knevels, E., Coulon, C., Segura, I., Haddick, P.C.G., Aerts, L., Delattin, N.,
701 Strasser, G., Oh, W.-J., Lange, C., Vinckier, S., Haigh, J., Fouquet, C., Henderson, C., Gu, C., Alitalo, K., Castellani,
702 V., Tessier-Lavigne, M., Chedotal, A., Charron, F., and Carmeliet, P. (2011). VEGF mediates commissural axon
703 chemoattraction through its receptor Flk1. Neuron *70*, 966–978.

704 Rutishauser, U., Acheson, A., Hall, A.K., Mann, D.M., and Sunshine, J. (1988). The neural cell adhesion molecule
705 (NCAM) as a regulator of cell-cell interactions. Science *240*, 53–57.

706 Rutishauser, U. (2008). Polysialic acid in the plasticity of the developing and adult vertebrate nervous system.
707 Nature reviews. Neuroscience *9*, 26–35.

708 Sassetti, C., van Zante, A., and Rosen, S.D. (2000). Identification of endoglycan, a member of the
709 CD34/podocalyxin family of sialomucins. JBC *275*, 9001–9010.

710 Schindelin, J., Arganda-Carreras, I., Frise, E., Kaynig, V., Longair, M., Pietzsch, T., Preibisch, S., Rueden, C.,
711 Saalfeld, S., Schmid, B., Tinevez, J.Y., White, D.J., Hartenstein, V., Eliceiri, K., Tomancak, P. and Cardona, A. Fiji:
712 an open-source platform for biological-image analysis. Nature Methods *9*, 676-682.

713 Short, C.A., Suarez-Zayas, E.A., and Gomez, T.M. (2016). Cell adhesion and invasion mechanisms that guide
714 developing axons. Curr. Opin. Neurobiol. *39*, 77–85.

715 Stoeckli, E.T., and Landmesser, L.T. (1995). Axonin-1, Nr-CAM, and Ng-CAM play different roles in the in vivo
716 guidance of chick commissural neurons. Neuron *14*, 1165–1179.

717 Stoeckli, E.T., Sonderegger, P., Pollerberg, G.E., and Landmesser, L.T. (1997). Interference with axonin-1 and
718 NrCAM interactions unmasks a floor-plate activity inhibitory for commissural axons. Neuron *18*, 209–221.

719 Stoeckli, E. (2017). Where does axon guidance lead us? F1000Research *6*.

720 Stoeckli, E.T. (2018). Understanding axon guidance. Are we nearly there yet? Development *145*.

721 Takeda, T., Go, W.Y., Orlando, R.A., and Farquhar, M.G. (2000). Expression of podocalyxin inhibits cell-cell
722 adhesion and modifies junctional properties in Madin-Darby canine kidney cells. Mol. Biol. Cell *11*, 3219–3232.

723 Tang, J., Rutishauser, U., and Landmesser, L. (1994). Polysialic acid regulates growth cone behavior during
724 sorting of motor axons in the plexus region. Neuron *13*, 405–414.

Vitureira, N., McNagny, K., Soriano, E., and Burgaya, F. (2005). Pattern of expression of the podocalyxin gene in the mouse brain during development. Gene Expr. Patterns *5*, 349–354.

Vitureira, N., Andrés, R., Pérez-Martínez, E., Martínez, A., Bribián, A., Blasi, J., Chelliah, S., López-Doménech, G., Castro, F. de, Burgaya, F., McNagny, K., and Soriano, E. (2010). Podocalyxin is a novel polysialylated neural adhesion protein with multiple roles in neural development and synapse formation. PloS one *5*, e12003.

Wallace, V.A. (1999). Purkinje-cell-derived Sonic hedgehog regulates granule neuron precursor cell proliferation in the developing mouse cerebellum. Curr. Biol. *9*, 445–448.

Wechsler-Reya, R.J., and Scott, M.P. (1999). Control of neuronal precursor proliferation in the cerebellum by Sonic Hedgehog. Neuron *22*, 103–114.

Wilson, N.H., and Stoeckli, E.T. (2011). Cell type specific, traceable gene silencing for functional gene analysis during vertebrate neural development. Nucleic Acids Res. *39*, e133.

Wilson, N.H., and Stoeckli, E.T. (2012). In ovo Electroporation of miRNA-based Plasmids in the Developing Neural Tube and Assessment of Phenotypes by DiI Injection in Open-book Preparations. Journal of Visualized Experiments : JoVE pii: 4384. doi: 10.3791/4384

Wilson, N.H., and Stoeckli, E.T. (2013). Sonic hedgehog regulates its own receptor on postcrossing commissural axons in a glypican1-dependent manner. Neuron *79*, 478–491.

Yaginuma, H., Homma, S., Künzi, R., and Oppenheim, R.W. (1991). Pathfinding by growth cones of commissural interneurons in the chick embryo spinal cord. A light and electron microscopic study. J. Comp. Neurol. *304*, 78–102.

Yam, P.T., Langlois, S.D., Morin, S., and Charron, F. (2009). Sonic hedgehog guides axons through a noncanonical, Src-family-kinase-dependent signaling pathway. Neuron *62*, 349–362.

Yam, P.T., Kent, C.B., Morin, S., Farmer, W.T., Alchini, R., Lepelletier, L., Colman, D.R., Tessier-Lavigne, M., Fournier, A.E., and Charron, F. (2012). 14-3-3 proteins regulate a cell-intrinsic switch from sonic hedgehog-mediated commissural axon attraction to repulsion after midline crossing. Neuron *76*, 735–749.

Zou, Y., Stoeckli, E., Chen, H., and Tessier-Lavigne, M. (2000). Squeezing axons out of the gray matter. A role for slit and semaphorin proteins from midline and ventral spinal cord. Cell *102*, 363–375.

755 **FIGURES**

756

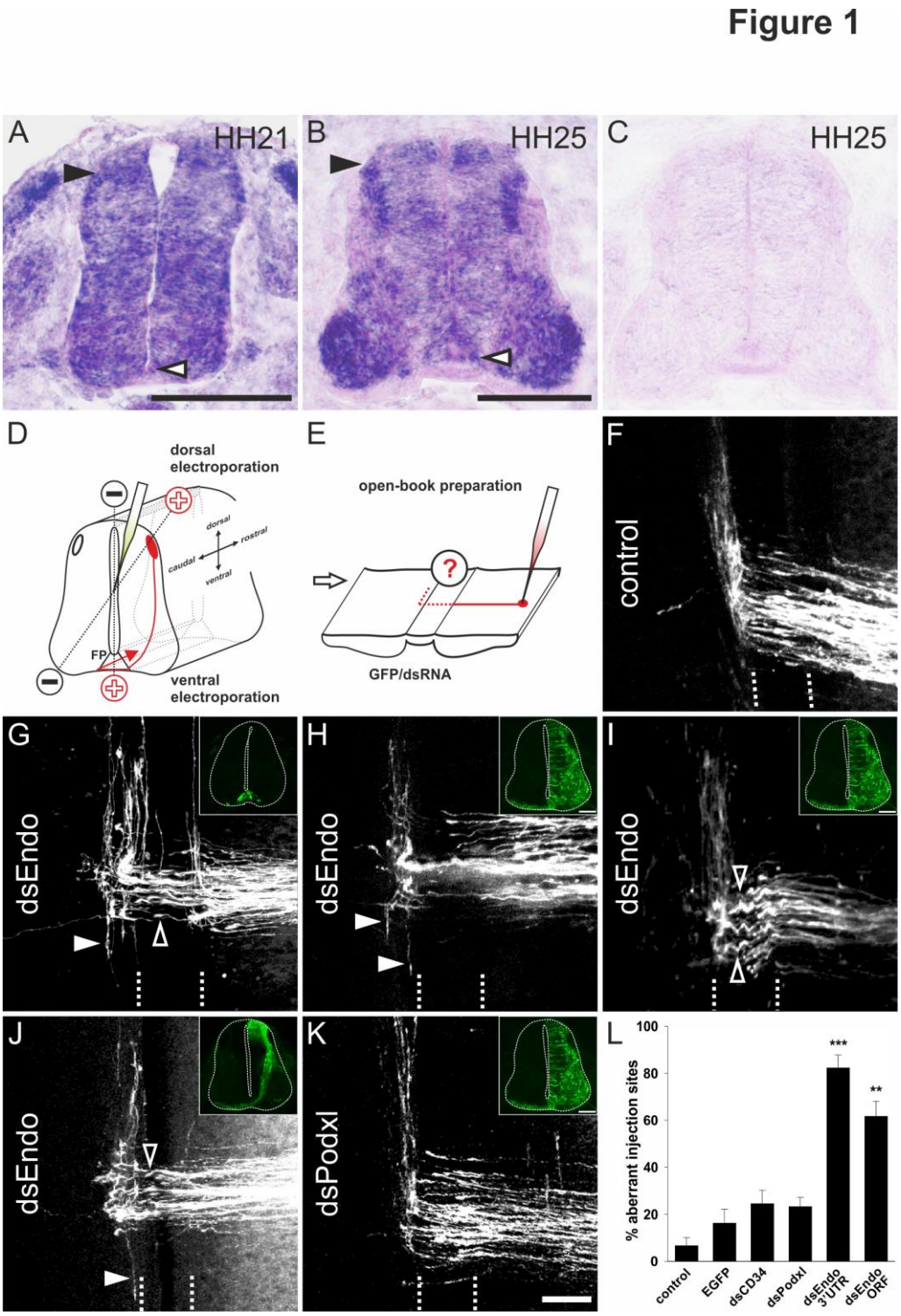

757

758

759 Figure 1

760 **Endoglycan is required for correct turning of post-crossing commissural axons**.

761 (A,B) *Endoglycan* is expressed in the developing neural tube during commissural axon guidance. *Endoglycan* is
762 expressed throughout the neural tube at HH21, including the floor plate (white arrowhead) (A). (B) At HH25,
763 *Endoglycan* is still found in most cells of the spinal cord. High levels are found in motoneurons and
764 interneurons, including the dorsal dI1 neurons (black arrowhead), and in the floor plate (white arrowhead). No
765 staining was found when hybridization was carried out with a sense probe (C). Commissural axon pathfinding
766 was analyzed in "open-book" preparations (D,E; see Methods for details). The positions of the electrodes for
767 dorsal and ventral electroporation are indicated (D). In control embryos at HH26, commissural axons have
768 crossed the floor plate and turned rostrally along the contralateral floor-plate border (F). In contrast, after
769 downregulation of Endoglycan (G-J) commissural axons failed to turn along the contralateral floor-plate border
770 or they turned randomly either rostrally or caudally (arrowheads in G-J). Occasionally axons were turning
771 already inside the floor plate (open arrowhead in G). A closer look at the morphology of the axons in the floor
772 plate revealed their tortuous, 'corkscrew-like' trajectory across the midline at many DiI injection sites (open
773 arrowheads in I).
774 To knockdown *Endoglycan* either in the floor plate or in commissural neurons, the ventral or dorsal spinal cord
775 was targeted as indicated in (D) (see inserts in G and J, respectively). Phenotypes were the same as those
776 observed after targeting one half of the spinal cord including the floor plate (H,I). Pathfinding was normal in
777 embryos electroporated with dsRNA derived from *Podocalyxin* (K).
778 The quantification of injection sites with pathfinding errors after targeting the floor plate or one half of the
779 spinal cord is shown in (L). Pathfinding errors were seen only at 6.7±3.4% of the injection sites in untreated
780 control embryos (n=10 embryos, 45 injection sites). In control embryos injected and electroporated with the
781 *EGFP* plasmid alone, pathfinding errors were found at 16.2±6% of the injection sites (n=17 embryos, 92
782 injection sites). Injection and electroporation of dsRNA derived from *CD34* (24.6±5.8%, n=8 embryos, 80
783 injection sites) and *Podocalyxin* (23.3±3.9%, n=17 embryos, 147 injection sites) did not affect midline crossing
784 and turning behavior of commissural axons. In contrast, 82.3±5.6% (n=11 embryos, 65 sites) and 61.7±6.4%
785 (n=18, 161 sites) of the injection sites in embryos injected with dsRNA derived from the 3'-UTR or the ORF of
786 *Endoglycan*, respectively, showed aberrant pathfinding of commissural axons. P values ***<0.001 and **<0.01,
787 compared to EGFP-injected control groups. The two groups electroporated with dsRNA derived from
788 *Endoglycan* were not different from each other. Values represent average percentage of DiI injection sites per
789 embryo with aberrant axonal navigation ± standard error of the mean. Bar: 50 µm.

790

Figure 2

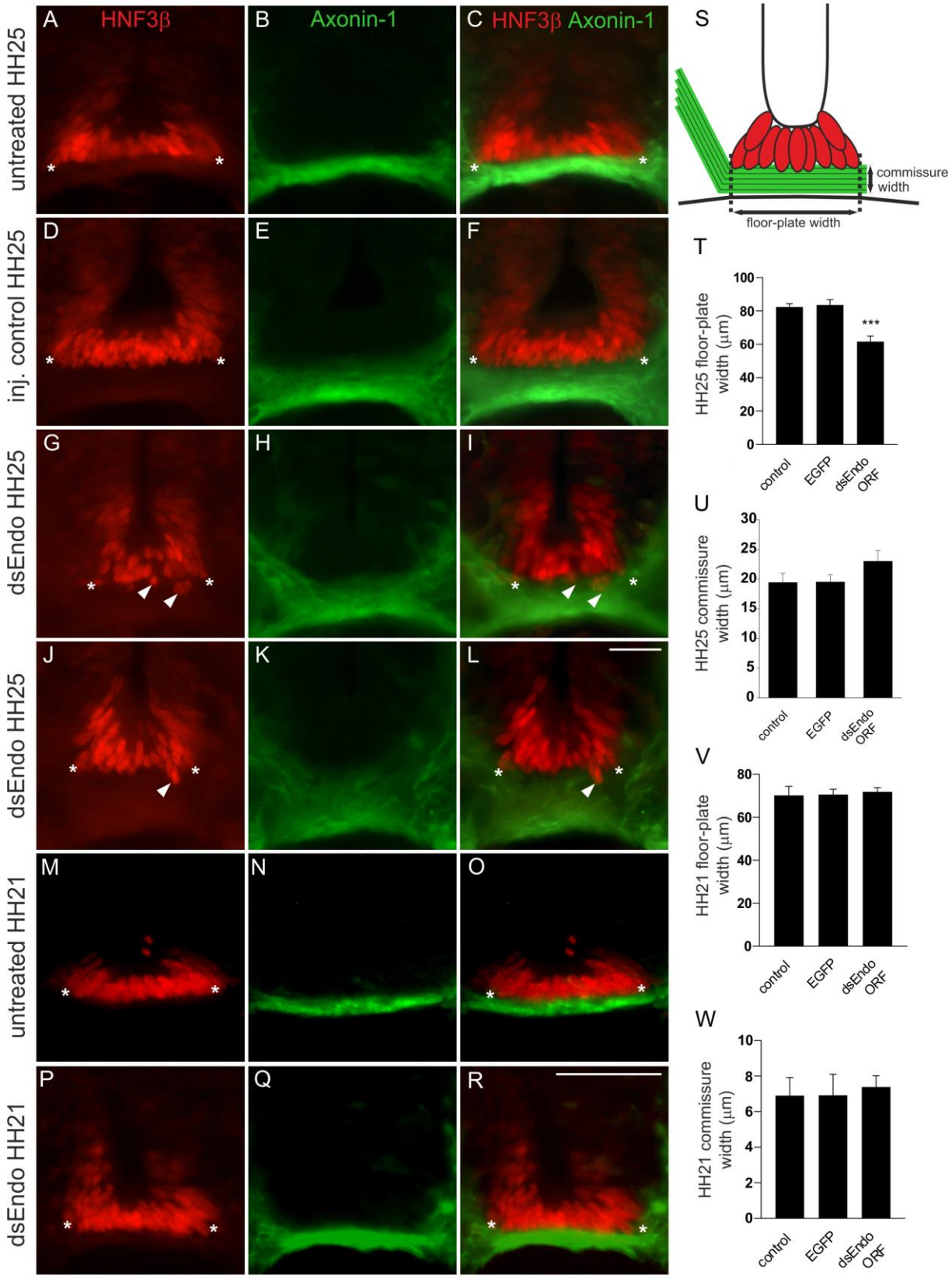

791

Figure 2

After downregulation of Endoglycan the floor-plate morphology is compromised only after axonal midline crossing.

In untreated (A-C) and control-treated embryos (D-F) the floor plate is of triangular shape with floor-plate cells precisely aligned at the ventral border. There is no overlap between the floor plate (visualized by HNF3β staining; red) and the commissure (visualized by anti-Axonin1 staining; green). The shape of the floor plate is no longer triangular in embryos lacking Endoglycan (G-L). The floor-plate cells are not aligned ventrally (arrowheads in G, I, J, and L) and the floor plate appears to have gaps. This change in morphology is only seen at HH25, when midline crossing is completed. When the floor-plate morphology was analyzed at HH21, there was no difference between control (M-O) and experimental embryos electroporated with dsRNA derived from *Endoglycan* (P-R). Note that some more ventral commissural axon populations have crossed the floor plate at this stage. But overall, the number of axons that form the commissure at HH21 is still very small. The width of the floor plate (indicated by asterisks) was measured (S,T). There was no significant difference in spinal cord width at HH25 (400.2±54.5 µm in untreated controls, 438.2±30.3 µm in EGFP-expressing controls, and 394±12.0 µm in dsEndo embryos), but floor plates were significantly narrower in embryos lacking Endoglycan (T; 61.6±3.4 µm; n=7 embryos; $p<0.001$) compared to untreated (82.4±2.0 µm; n=6 embryos) and *EGFP*-injected control embryos (83.6±3.2 µm; n=6 embryos). The commissure had a tendency to be wider in experimental compared to control embryos but the effect was not statistically significant (U). The width of the floor plate was not different between groups when measured at HH21 (V) with 70.1±4.2 µm (n=3) for untreated and 70.6±2.5 µm for EGFP controls (n=4), compared to 71.8±2.0 µm for experimental embryos (n=3). No difference was seen in the width of the commissure. Bar: 50 µm. ANOVA with Bonferroni correction was used for statistical analyses.

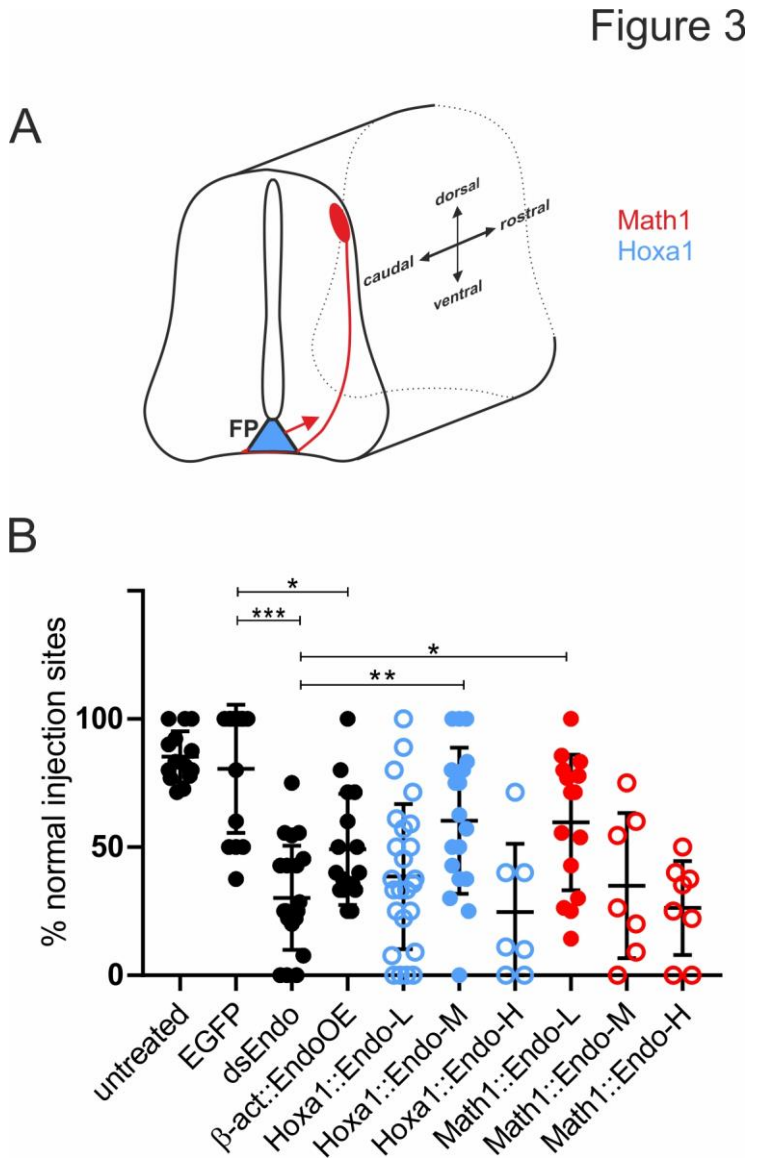

Figure 3

Too much or too little Endoglycan causes aberrant axon guidance

Because silencing *Endoglycan* either in commissural neurons or in the floor plate caused the same type of axon guidance defects, we wanted to test the idea that the presence of an adequate amount, but not the source of Endoglycan was important. We therefore downregulated Endoglycan by transfection of dsRNA derived from the 3'UTR of *Endoglycan* into one half of the spinal cord. We then tried to rescue the aberrant axon guidance phenotype by co-electroporation of the *Endoglycan* ORF specifically in dI1 neurons (using the Math1 enhancer, red) or in the floor plate (using the Hoxa1 enhancer; blue, A). The rescue constructs were used at a concentration of 150 (L = low), 300 (M = medium), and 750 (H = high) ng/µl, respectively. In both cases, rescue was only possible with one concentration: the medium concentration of the Endoglycan plasmid driven by the Hoxa1 promoter and the low concentration of the plasmid driven by the Math1 promoter. The lowest

concentration of the Hoxa1-driven construct and the two higher concentrations of the Math1-driven constructs were not able to rescue the aberrant phenotype. Note that the amounts of Endoglycan cannot be compared between the Math1- and the Hoxa1 enhancers, as they differ in their potency to drive expression. However, we can conclude a response in a dose-dependent manner in both cases. Statistical analysis by one-way ANOVA: *$p<0.05$, **$p<0.01$, ***$p<0.001$. See Table 1 for quantification.

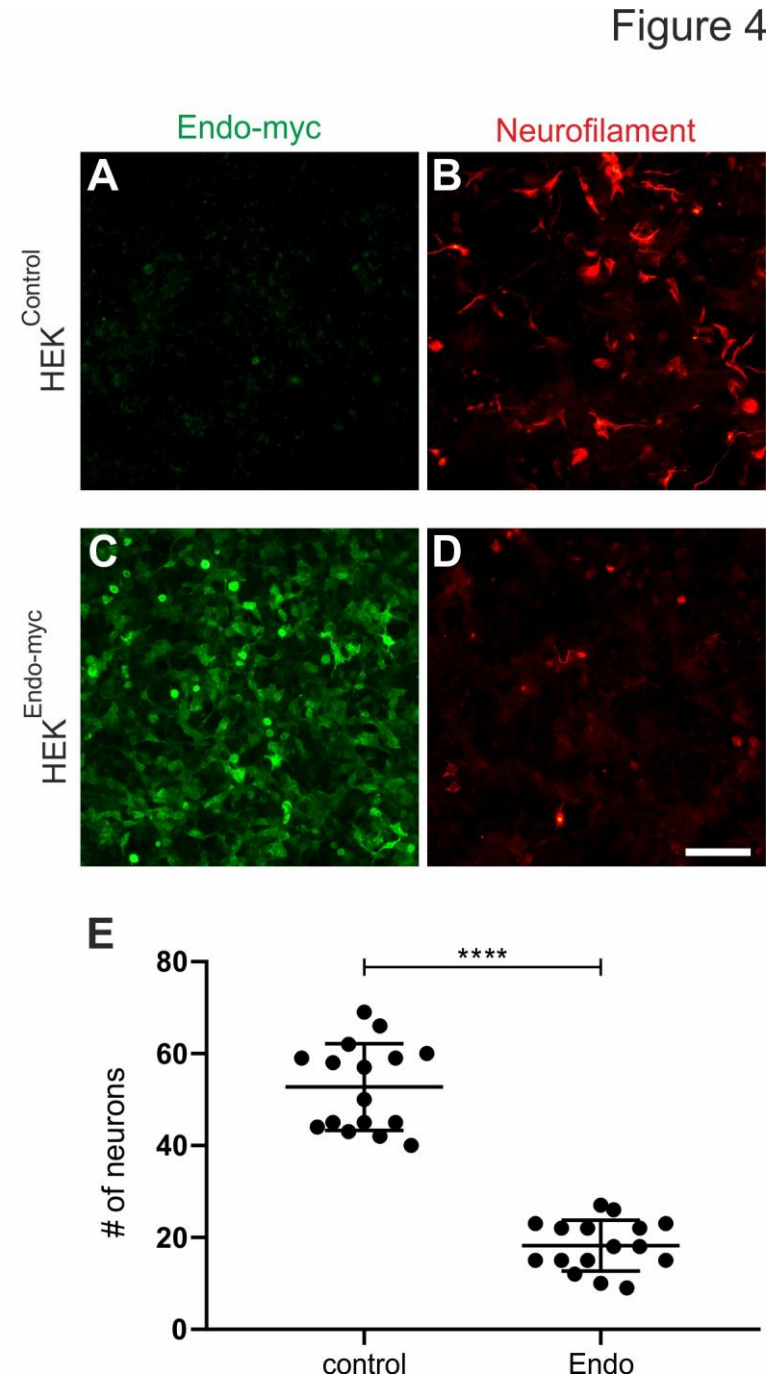

Figure 4

Endoglycan expression reduces cell adhesion in vitro

Control HEK cells (A) or HEK cells stably expressing human Endoglycan (C) were used as carpet for dissociated motoneurons dissected from HH26 chicken embryos (B,D). Neurons were allowed to attach for 40 hours. Staining for Neurofilament revealed a pronounced decrease in the number of motoneurons on HEK cells expressing Endoglycan (D) compared to control HEK cells (B). On control HEK cells (A), we found 52.8±2.4

motoneurons per view field. On a carpet of HEK cells expressing Endoglycan only 18.3±1.4 motoneurons were counted. Similar results were obtained in five independent experiments. Bar: 100 µm. ****$p<0.0001$, unpaired t test, two-tailed.

Figure 5

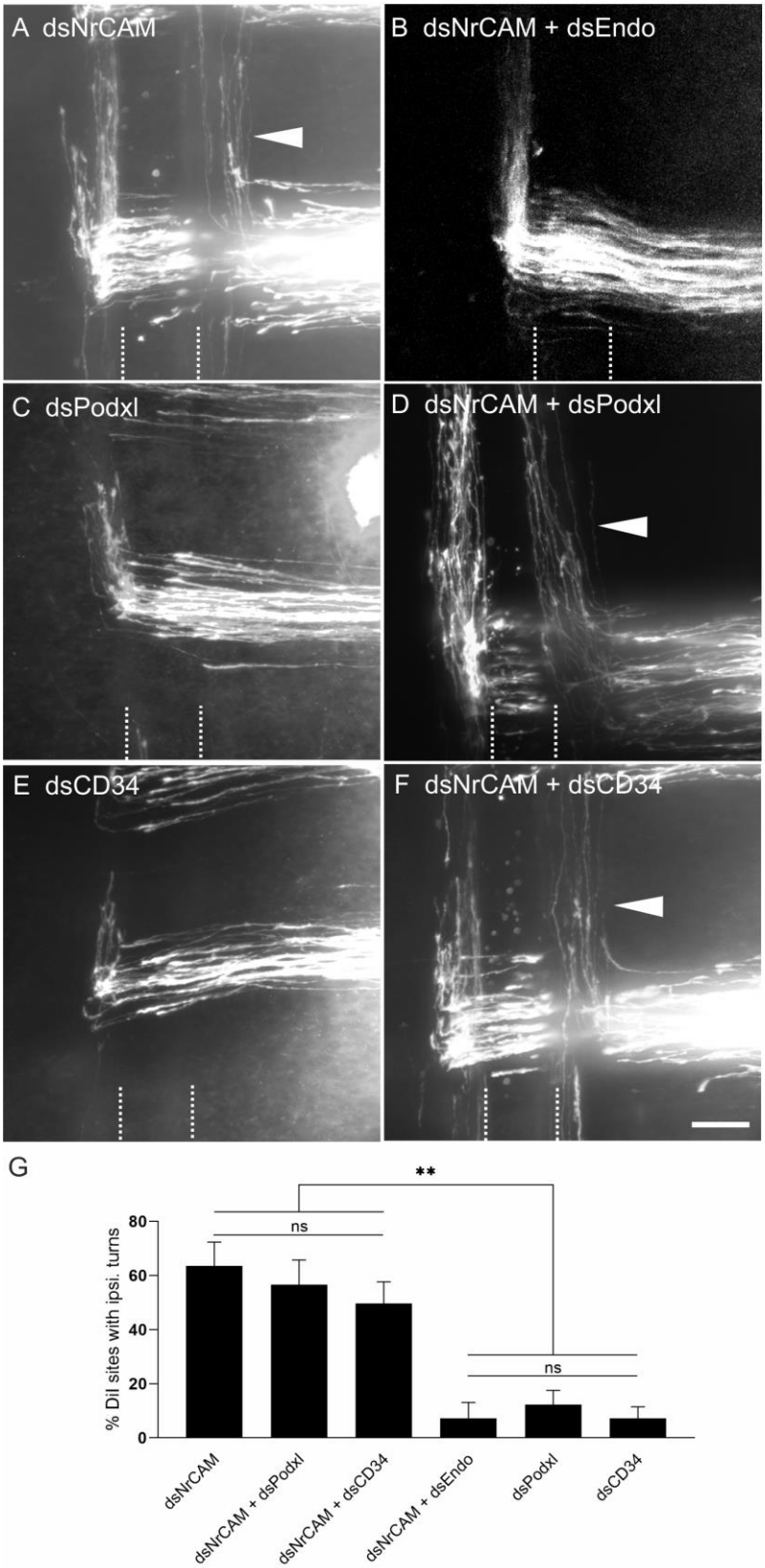

854

855

856

857 Figure 5

858 **Downregulation of Endoglycan but not its family members rescues the axon guidance phenotype induced by**
859 **downregulation of NrCAM**

860 The perturbation of axon/floor-plate contact by downregulation of NrCAM resulted in the failure of
861 commissural axons to enter the floor-plate area and caused their premature turns along the ipsilateral floor-
862 plate border (arrowhead in A) at 63.6±8.8% of the injection sites (n=7 embryos, 90 injection sites; G). These
863 results are in line with previous reports (Stoeckli and Landmesser, 1995; Philipp et al., 2012). When both
864 NrCAM and Endoglycan were downregulated, the number of ipsilateral turns was reduced to control levels
865 (B,G; 7.3±5.8%, n=10 embryos; 78 injection sites), consistent with the idea that a decrease in adhesion due to a
866 lack of NrCAM can be balanced by an increase in adhesion between floor plate and growth cones due to a lack
867 of Endoglycan. Downregulation of either Podocalyxin (C) or CD34 (E) did not impair axon guidance (see also
868 Figure 1; 12.3±5.2% (n=9) and 7.25±4.3% (n=8), respectively). In contrast to Endoglycan, neither concomitant
869 downregulation of Podocalyxin (D) nor CD34 (F) could rescue the NrCAM-induced ipsilateral turns, as aberrant
870 axon behavior was still observed at 56.7±9.2% (n=8 embryos, 77 injection sites) and 49.6±8.1% (n=10 embryos,
871 100 injection sites), respectively. The floor plate is indicated by dashed lines. For statistical analysis, one-way
872 ANOVA followed by Tukey's multiple comparisons test was used, ** $p<0.01$; (ns) $p\geq0.05$. Bar: 50 µm.

873

Figure 6

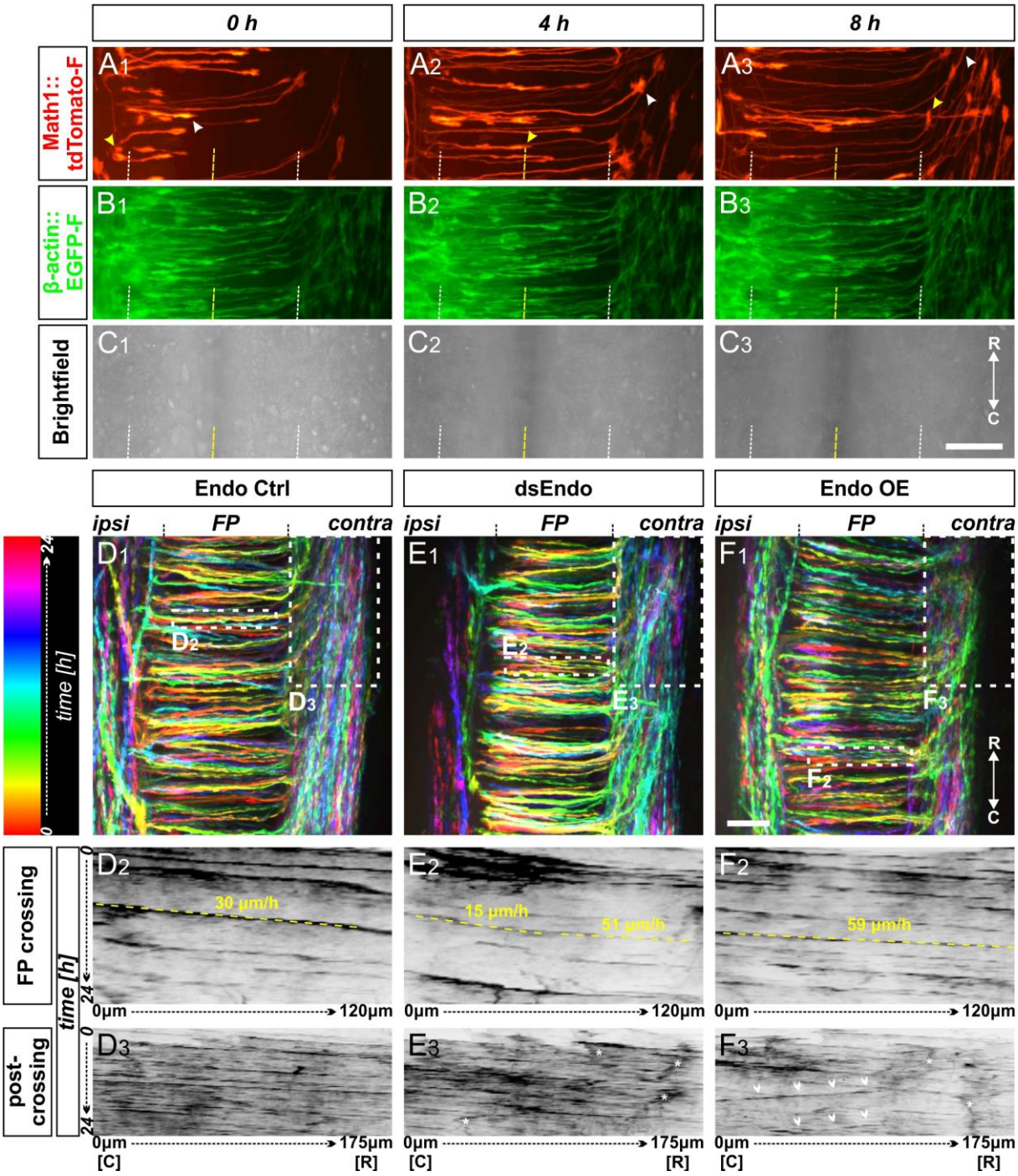

Figure 6

Live imaging of cultured intact spinal cords revealed major impacts of different Endoglycan levels on midline crossing

(A-C) Live imaging allowed tracing and quantitative analysis of dI1 axons' trajectories in cultured intact chicken spinal cords. (A_{1-3}) The behavior and trajectory of single tdTomato-positive dI1 axons could be tracked over

880 time when they crossed the floor plate and turned rostrally (yellow and white arrowheads). (B-C) EGFP-F
881 expression under the β-actin promoter and brightfield images helped to visualize the floor plate boundaries
882 (white dashed line) and the midline (yellow dashed line). (D_1, E_1, F_1) Temporally color-coded projections of 24h
883 time-lapse movies (Supplementary movie 1). Kymograph analysis of the regions of interest selected in the floor
884 plate of each condition shown in (D_1,E_1,F_1) was used to calculate growth cone speed during floor-plate crossing
885 (D_2, E_2, F_2) and after turning into the longitudinal axis (D_3, E_3, F_3). Yellow dashed lines outline a representative
886 example of the slope (velocity) of a single axon crossing the floor plate in each condition. TdTomato-positive
887 axons in control-injected spinal cords (D_{1-3}) crossed the floor plate at a steady speed of 30 µm/h (D_2) and
888 turned rostrally in a highly organized manner (D_3). In contrast, growth cone speed in the first half of the floor
889 plate that was electroporated with dsRNA derived from Endoglycan (dsEndo) was markedly slowed down to
890 only 15 µm/h. In the second, non-electroporated half of the floor plate, axons electroporated with dsEndo
891 were faster than control axons (51 µm/h; E_2). Axons overexpressing Endoglycan were faster in both halves of
892 the floor plate (59 µm/h; F_2). Downregulation or overexpression of Endoglycan clearly impacted the rostral
893 turning behavior visualized by less organized patterns (D_3-F_3). Asterisks mark axons stalling and thus causing a
894 'smeared' pattern in the kymographs. Arrowheads indicate caudally turning axons. R, rostral; C, caudal; ipsi,
895 ipsilateral; contra, contralateral; FP, floor plate. Scale bars: 50 µm.
896

Figure 7

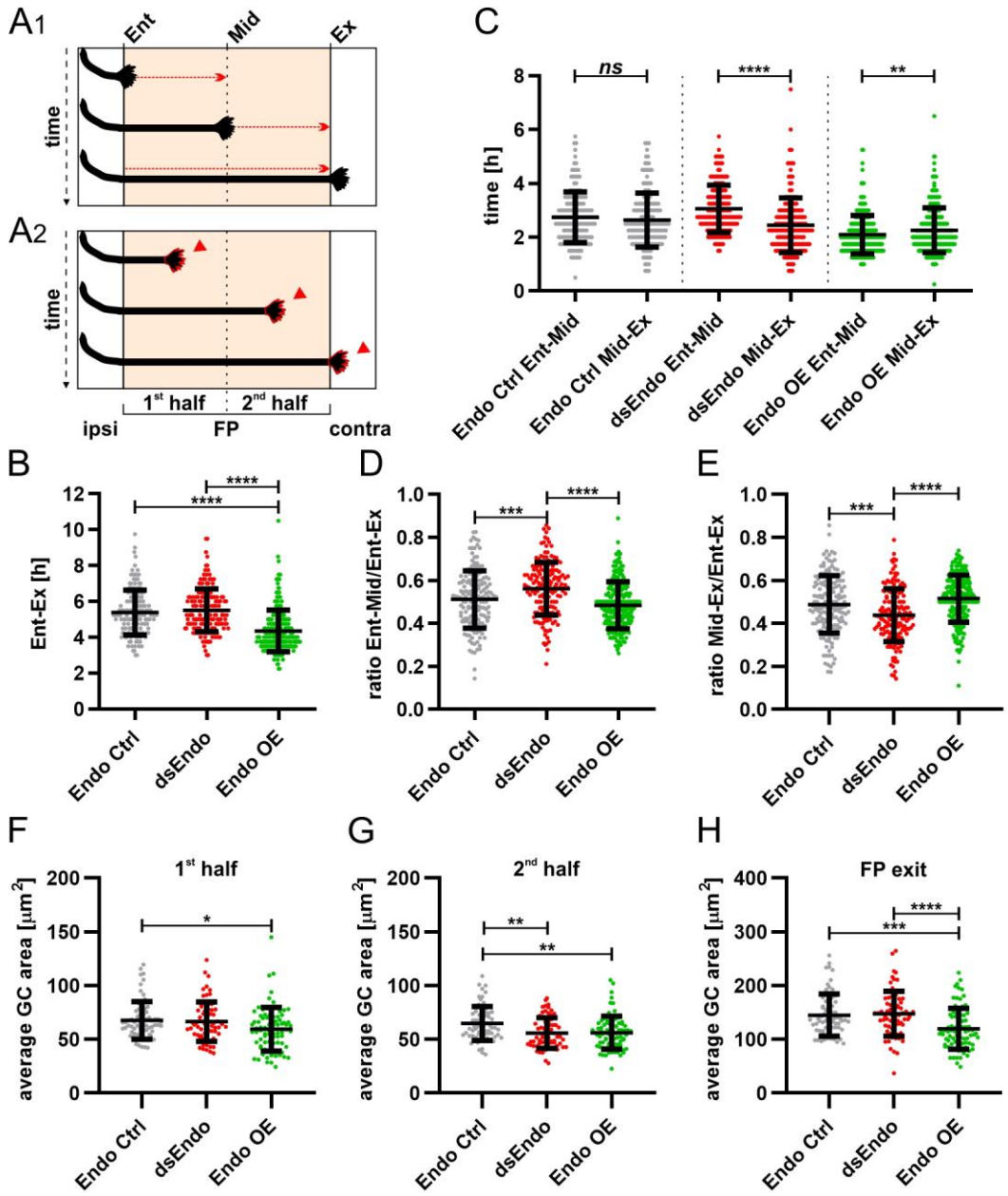

Figure 7

Too much or too little of Endoglycan impaired the timing and morphology of single dI1 growth cones migrating in the floor plate

Data at the single axon level extracted from 24h time-lapse recordings of tdTomato-positive dI1 axons crossing the floor plate. (A_1) The time of floor-plate crossing was measured for the entire floor plate, for the first and for the second half for each condition. (A_2) The average growth cone area was measured in the first half, the second half and at the exit site of the floor plate for each condition. (B) Overexpression of *Endoglycan*

906 significantly decreased the time axons needed to cross the entire floor plate compared to control and dsEndo
907 conditions (Kruskal-Wallis test with Dunn's multiple-comparisons test). (C) The average time of crossing the
908 first half and the second half of the floor plate was compared. Interestingly, there was a highly significant
909 difference in the spinal cords unilaterally electroporated with dsEndo, as axons spent much longer in the first
910 compared to the second half of the floor plate. There was no difference between the two halves of the floor
911 plate in the control condition, but there was a significant decrease in growth cone speed between the first
912 (electroporated) half of the floor plate and the second half, where only axons were overexpressing *Endoglycan*
913 (Wilcoxon test). (D) and (E) The ratios of the time axons spent in the first half (D) or the second half (E) of the
914 floor plate divided by the time they needed to cross it entirely were compared between conditions. Unilateral
915 knockdown of Endoglycan resulted in a significant increase of the ratio in the first half and a decrease in the
916 second half compared to both control and overexpression conditions (one-way ANOVA with Sidak's multiple-
917 comparisons test). (F-H) The average dI1 growth cone area at each position of the floor plate (as depicted in A_2)
918 were compared across all conditions. (F) Overexpression of Endoglycan induced a significant reduction in the
919 average growth cone area compared to the control condition (Kruskal-Wallis test with Dunn's multiple-
920 comparisons test) but not compared to Endoglycan knockdown (*p* value = 0.08). (G) In the second half of the
921 floor plate the average growth cone area was reduced in both Endoglycan knockdown and overexpression
922 compared to control (one-way ANOVA with Sidak's multiple-comparisons test). (H) At the floor plate exit site,
923 overexpression of *Endoglycan* induced a significant decrease in the average growth cone area compared to
924 both control and knockdown conditions (one-way ANOVA with Sidak's multiple-comparisons test). Error bars
925 represent standard deviation. $p<0.0001$ (****), $p<0.001$ (***), $p<0.01$ (**), $p<0.05$ (*) and $p\geq0.05$ (ns) for all
926 tests. See Table 2 for detailed results. Ent, entry; Mid, midline; Ex, exit; ipsi, ipsilateral; contra, contralateral; FP,
927 floor plate; GC, growth cone.
928

Figure 8

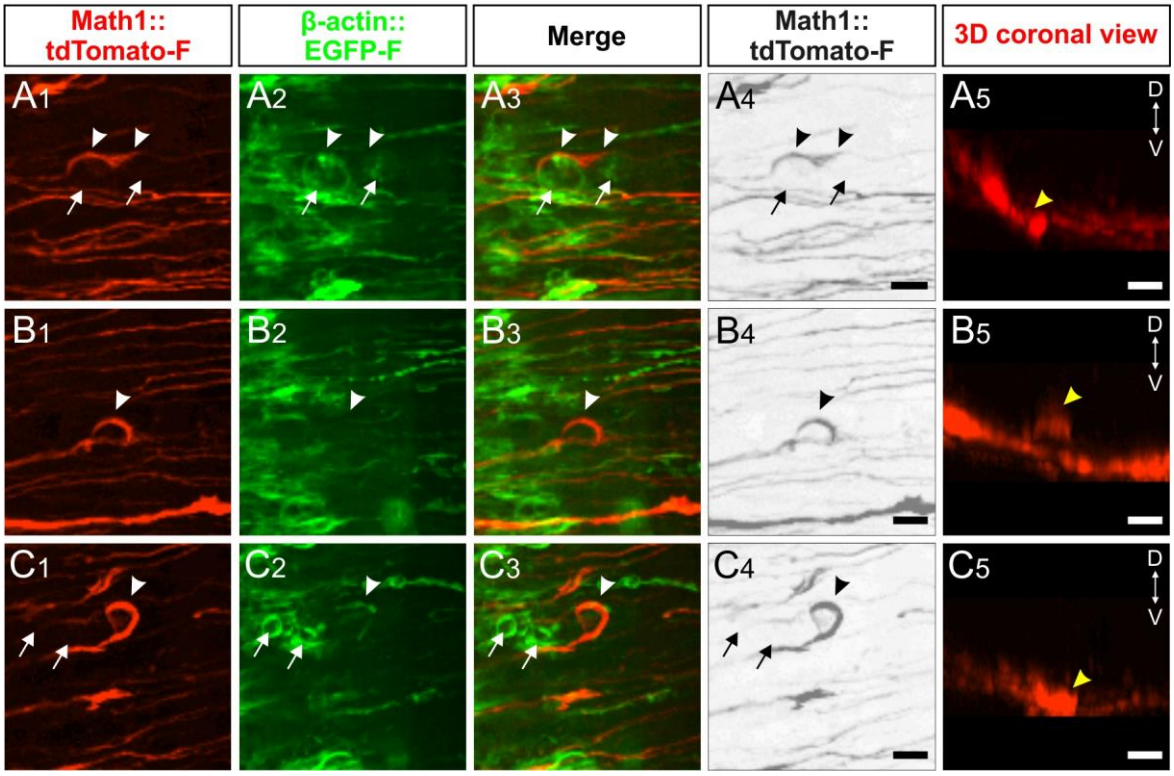

Figure 8

Live imaging of dI1 axons after perturbation of Endoglycan expression explains 'corkscew-like' phenotypes by aberrant interactions between axons and floor-plate cells

(A-C) ´Corkscrew´-like phenotypes of dI1 axons expressing farnesylated tdTomato were observed by live imaging in the first half of the floor plate (electroporated half) only after *Endoglycan* was silenced (see also Supplementary movies 4 and 5). (A) Dislocated EGFP-positive cells (arrows) caused dI1 axons to deviate from a smooth trajectory inducing a ´corkscrew-like´ morphology (arrowheads, A_{1-4}). These axons and cells were located in the commissure as shown in a coronal view (yellow arrowhead, A_5 and Supplementary movie 4). (B) Some axons were found to form a loop (arrowheads, B_{1-4}) invading the layer of the floor plate where somata of floor-plate cells are located as shown in the transverse view (yellow arrowheads, B_5 and Supplementary movie 5). (C) Clusters of dislocated roundish EGFP-positive cells (arrows) seemed to retain growth cones in the first half of the floor plate (arrowheads). These axons and cells were located in the commissure as shown in a coronal view (yellow arrowhead, C_5 and Supplementary movie 5). D, dorsal; V, ventral. Scale bars: 10 µm.

Figure 9

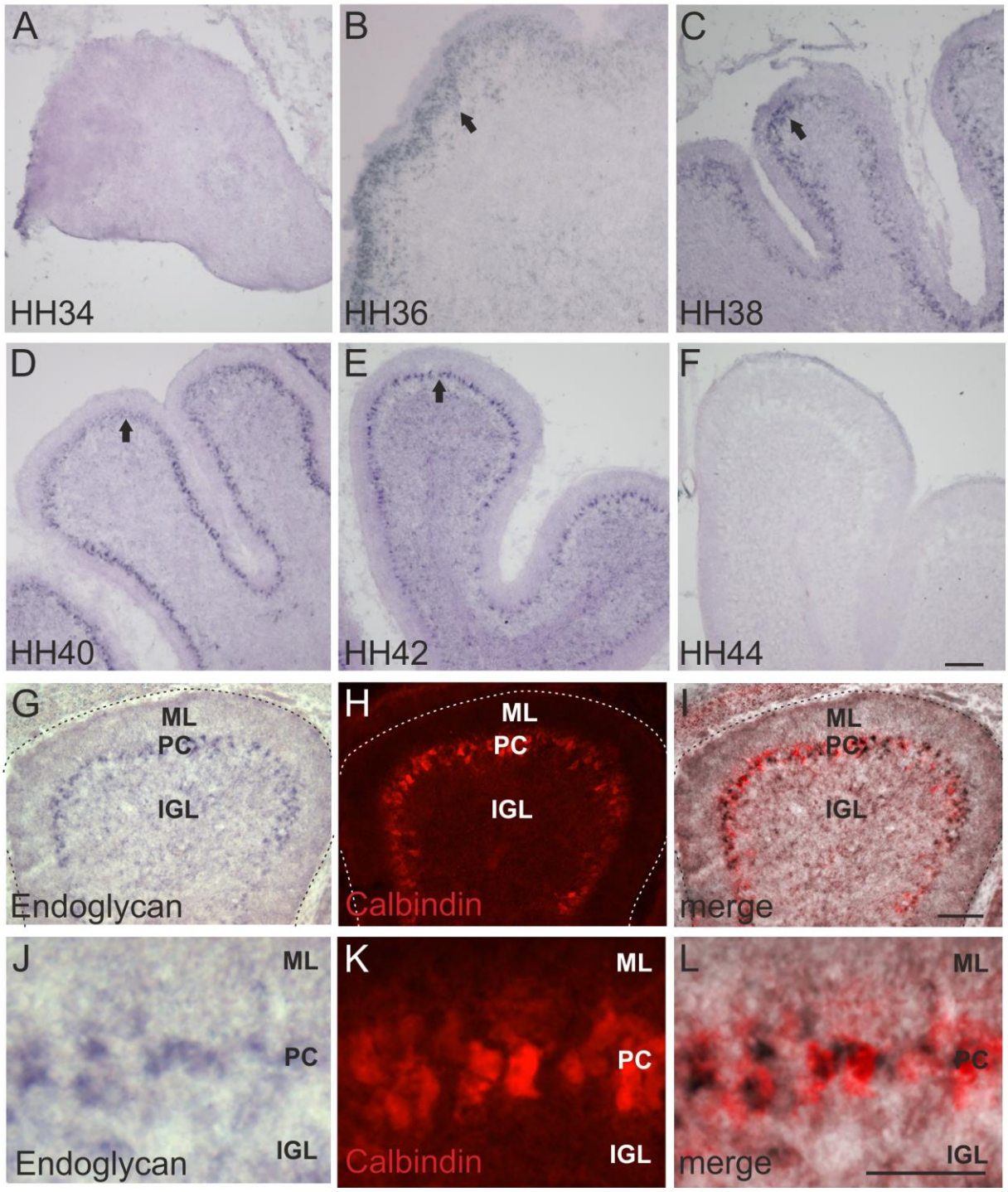

Figure 9

***Endoglycan* expression is restricted to Purkinje cells in the developing cerebellum**

The temporal analysis of *Endoglycan* expression in the developing cerebellum localized it to migrating Purkinje cells. No *Endoglycan* expression was found at HH34 (A). Starting at HH36 (B), *Endoglycan* mRNA was found in

migrating Purkinje cells. No change in expression was seen at HH38 (C), HH40 (D), and at HH42 (E) (arrows). At HH44, after migration of Purkinje cells was completed, *Endoglycan* was no longer expressed (F). We used Calbindin to identify Purkinje cells (H,K). At HH38, the in situ signal for *Endoglycan* (G,J) co-localized with Calbindin staining (H,K; overlay in I,L). Bar: 100 µm in A-F, 100 µm in G-I, 50 µm in J-L.

Figure 10

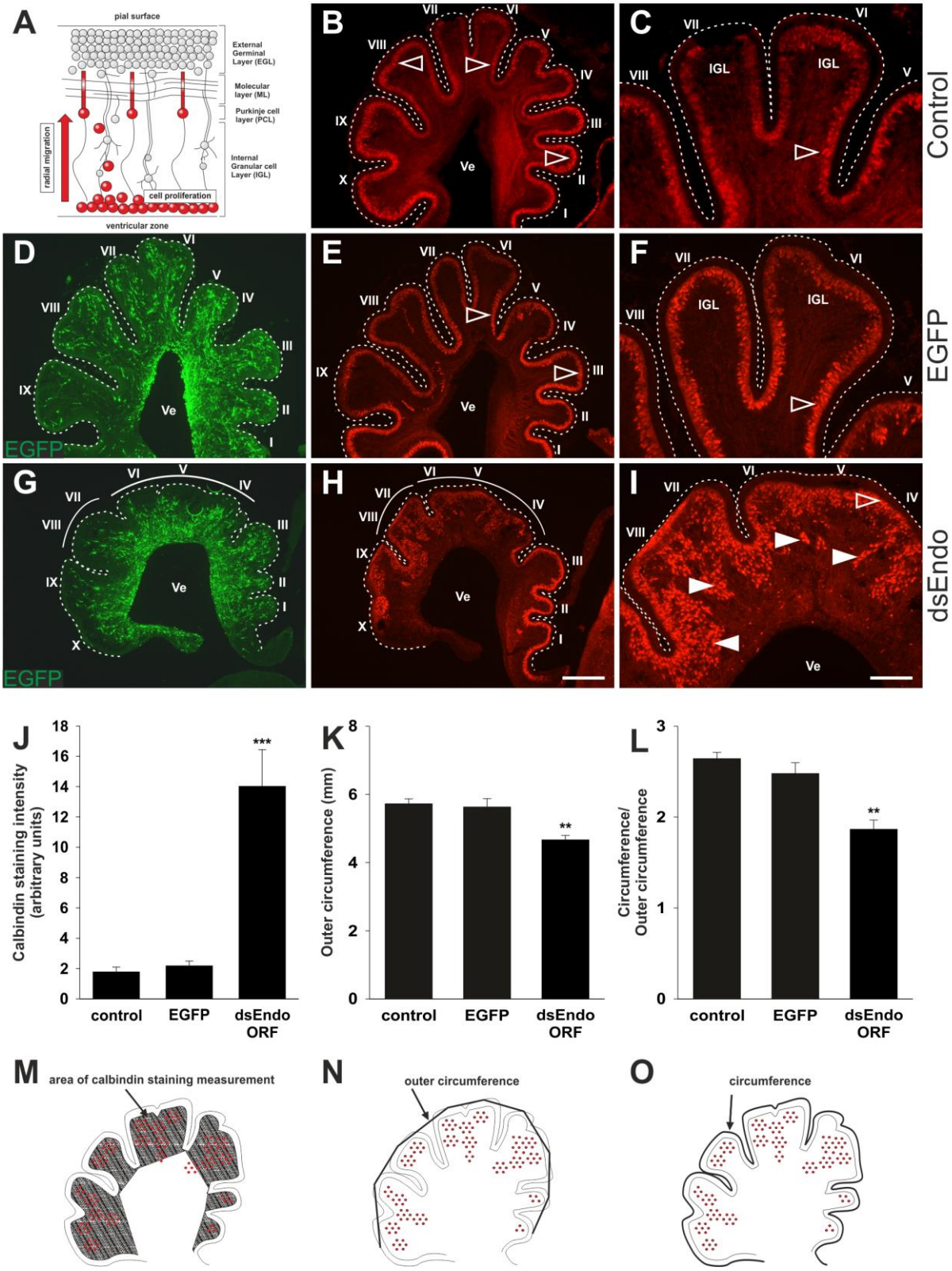

Figure 10

Endoglycan is required for Purkinje cell migration

960 Purkinje cells are born in the ventricular zone of the cerebellum. They migrate radially toward the periphery of
961 the cerebellar folds to form the Purkinje cell layer (A). In control embryos at HH38, the Purkinje cell layer
962 visualized by Calbindin staining is clearly detectable, although not fully matured to a monolayer (B and C).
963 Control-injected embryos (D-F) were not different from untreated control embryos. Calbindin stains Purkinje
964 cells in the periphery of the cerebellar folds (E and F). In the absence of Endoglycan (G-I) Purkinje cells failed to
965 migrate and remained stuck in the center of the cerebellar folds (H, arrowheads in I). The failure of Purkinje
966 cells to migrate radially was quantified by measuring fluorescence intensity for Calbindin in control (n=5
967 embryos), *EGFP*-injected (n=4 embryos), and *Endoglycan* dsRNA-treated embryos (J; n=5 embryos). Calbindin
968 staining intensity was measured as indicated in (M). The increase is highly significant for *Endoglycan* dsRNA-
969 treated embryos, $p < 0.001$. As a measure for the size of the cerebellum, the outer circumference was
970 measured as indicated in (N). The cerebellum was smaller in experimental embryos compared to both control
971 groups (K; $p<0.01$). In order to quantify the reduction in the number of folds that was obvious from the visual
972 inspection of cerebellar sections, we measured the actual circumference of the cerebellum as indicated in (O)
973 and divided it by the outer circumference. Control embryos had a ratio of 2.64±0.06 and 2.47±0.11,
974 respectively. Embryos lacking Endoglycan showed a clear reduction in the ratio between the two
975 circumferences with a value of 1.8±0.1 (L; $p<0.01$), indicating that they had fewer cerebellar folds compared to
976 control embryos, which had always 10 distinct folds. Bar: 500 µm in B, D, E, G, H; 200 µm in C, F, I. ANOVA with
977 Bonferroni post-hoc test was used for statistical analysis.
978

Figure 11

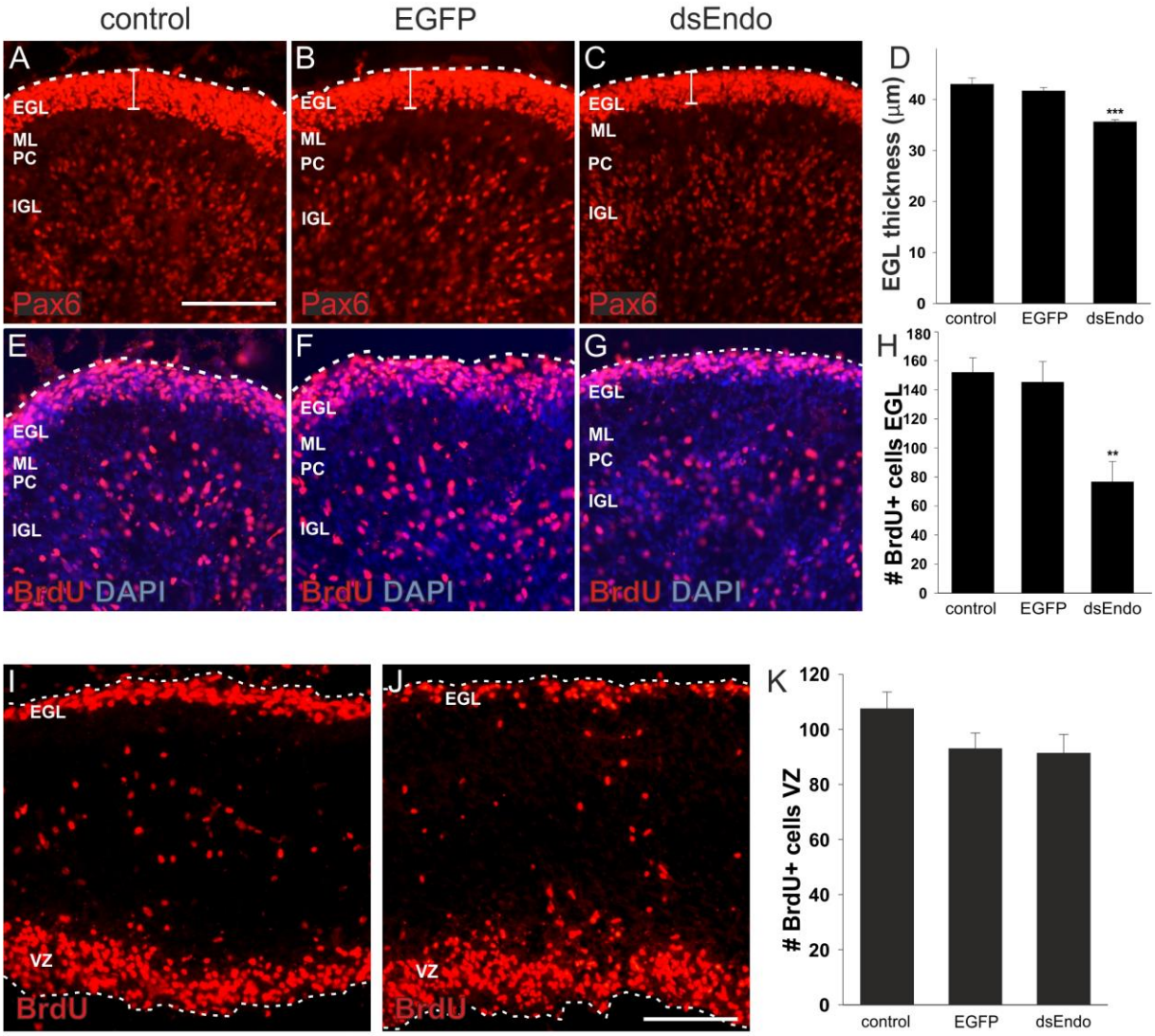

979

980

981 Figure 11

982 **Downregulation of Endoglycan results in a smaller cerebellum due to reduced proliferation of granule cells**.

983 The failure of Purkinje cell migration has negative consequences on granule cell proliferation (A-H). Granule

984 cells in the EGL and in the developing IGL are labeled by Pax6 (A-C). A reduction in the width of the EGL was

985 found for embryos treated with dsRNA derived from *Endoglycan* (C,D; n=3 embryos; $p<0.001$) compared to

986 age-matched untreated embryos (A; n=4 embryos), or control-treated embryos, expressing EGFP (B; n=3

987 embryos), when sections from the same relative position of the cerebellum were analyzed. No difference was

988 found between the two control groups (D). The proliferation of granule cells in the outer EGL was visualized by

BrdU incorporation (E-H). Embryos were exposed to BrdU for 3 hours before they were sacrificed at HH38. The number of BrdU-positive cells in the outer EGL was compared between untreated (E; n=6 embryos), EGFP-expressing control embryos (F; n=4 embryos) and embryos lacking Endoglycan (G; n=5 embryos). The number of BrdU-positive cells was significantly reduced in embryos lacking Endoglycan (H; $p<0.01$). The number of BrdU-positive cells in the ventricular zone at HH35 did not differ between untreated controls (I) and embryos lacking Endoglycan (J; K). The number of BrdU-positive cells in the ventricular zone is given per 10'000 μm^2. Bar: 100 µm. ANOVA with Bonferroni post-hoc test was used for statistical analysis.

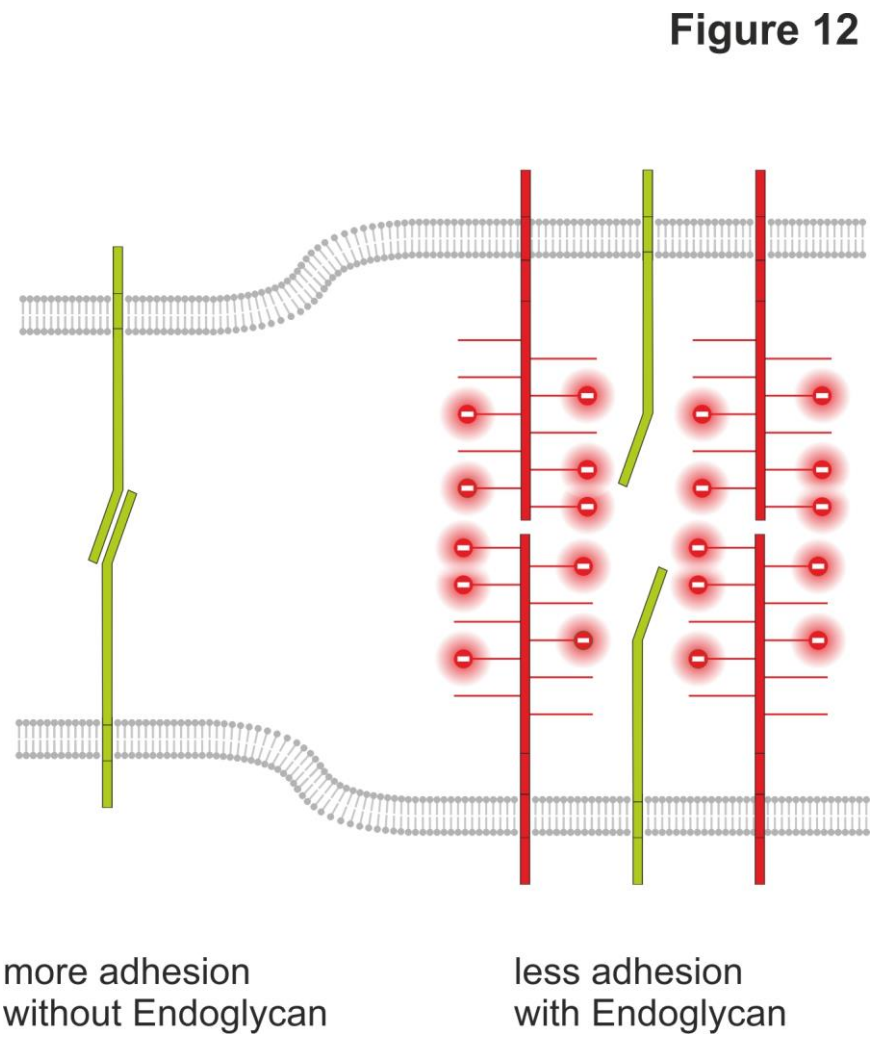

Figure 12

Endoglycan modulates cell-cell contact by interference with adhesive strength

Based on our in vivo and in vitro studies we postulate a model for Endoglycan function in neural circuit formation that suggests an 'anti-adhesive' role by modulation of many specific molecular interactions due to decreasing cell-cell contact. This model is consistent with our rescue experiments demonstrating that the source of Endoglycan did not matter but the expression level did, as aberrant phenotypes were prevented when Endoglycan was expressed either in the axon or in the floor plate.

Supplementary Figures

Supplementary Figure 1

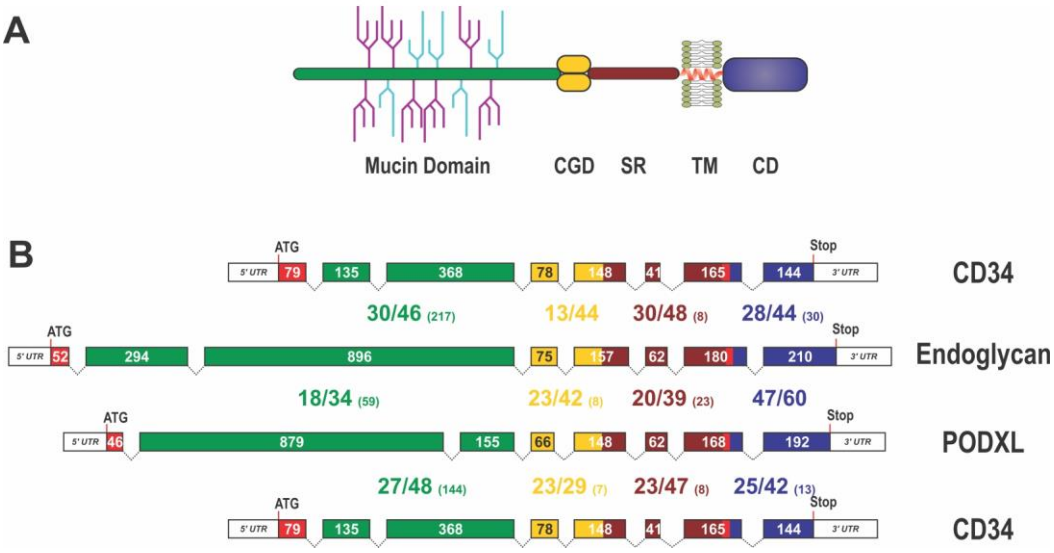

Supplementary Figure 1

Domain organization, exon alignment and conservation of the CD34 family of sialomucins

(A) Schematic drawing of the domain organization of CD34 family members. They all contain an N-terminal, highly glycosylated, mucin domain (green), a cysteine-containing globular domain (CGD, yellow), a juxtamembrane stalk region (SR, brown), as well as a transmembrane alpha-helix (TM, red) and a cytoplasmic domain (CD, blue). O-linked glycosylation sites within the mucin domain are depicted in light blue, whereas further sialylated residues are symbolized in purple. N-linked glycosylation sites are not shown. Note, that the indicated glycosylation sites in this scheme are only symbolizing the extensive amount of glycosylation in sialomucins and are not representing the actual position of glycosylation. (B) Exon organization and domain conservation of sialomucins. Transcripts of CD34 family members are encoded by eight separate exons (colored boxes). While the length of exons coding for the cysteine containing globular domain (yellow), the juxtamembrane stalk region (brown), and the cytoplasmic domain (blue) are more or less conserved (exon sizes are given within the boxes), exons coding for the mucin domain (green) vary markedly in their length and organization. The translational start sites are highlighted by the ATG and the end of the coding sequences are indicated by the given Stop codon. Protein homology between the different chicken sialomucins is depicted by the large numbers between the exon pictograms. All domains were compared separately and the colors used indicate the corresponding domains. The first number indicates identical amino acids between the compared

proteins, the second number represents conserved residues and the number in brackets designates the amount of gap positions within the alignment of the domains (eg. 28/44 (30)). The alignment was done using MUSCLE version 3.7. configured to the highest accuracy (Edgar, 2004). Single gap positions were scored with high penalties, whereas extensions of calculated gaps were less stringent. Using such parameters homologous regions of only distantly related sequences can be identified. Note, that within the mucin domain only some blocks, interspaced by sometimes large gap regions, are conserved between the different proteins.

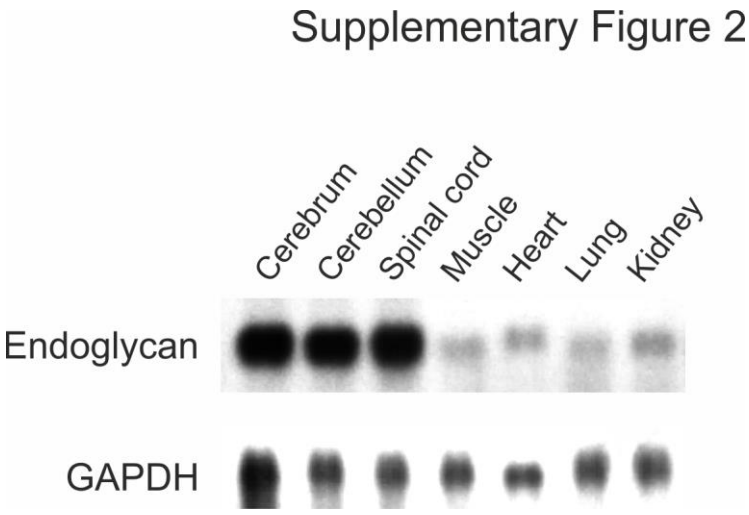

Supplementary Figure 2

Endoglycan is mainly expressed in the developing nervous system

Endoglycan is expressed only at low levels in non-neuronal tissues. Northern blot analysis of tissues taken from HH38 chicken embryos revealed its high expression levels in the cerebrum (brain without cerebellum), the cerebellum, and the spinal cord. Only low levels were found in muscle, heart, lung, and kidney. GAPDH was used as a loading control.

Supplementary Figure 3

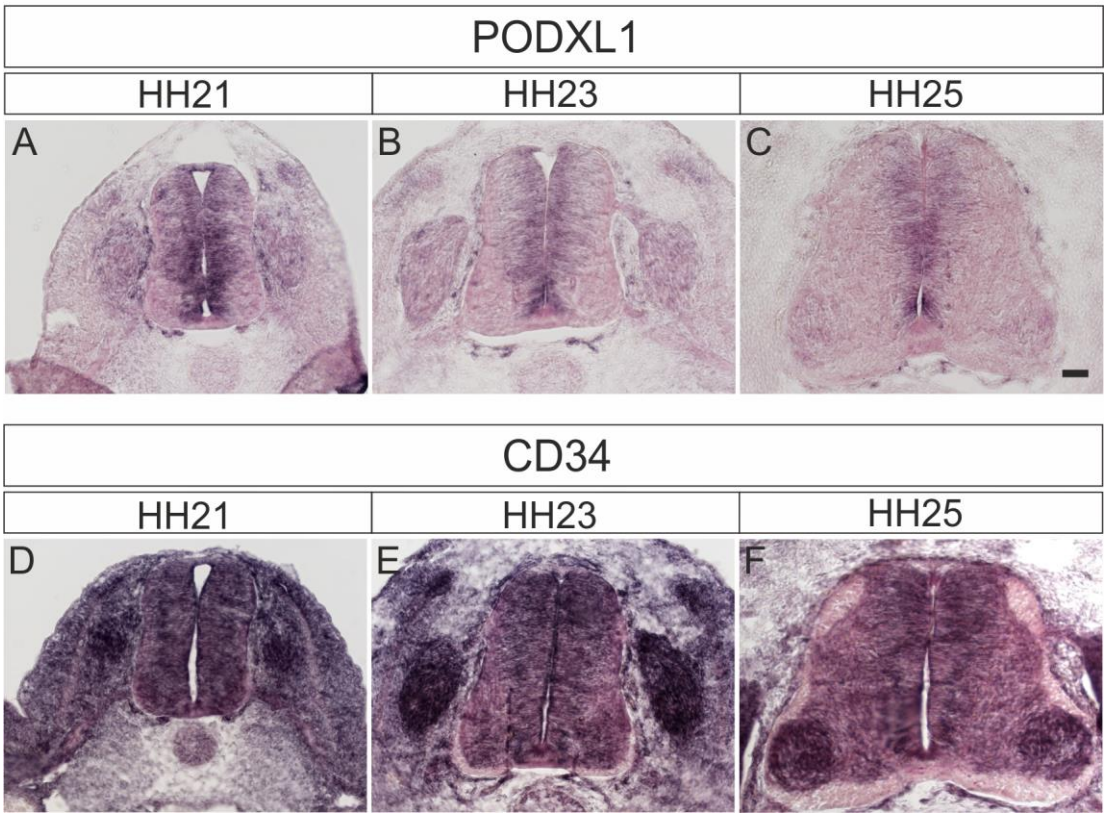

Supplementary Figure 3

Podocalyxin and CD34 are expressed in the developing spinal cord during midline crossing of dI1 commissural axons

Podocalyxin1 expression was mainly found in the ventricular zone (A-C). At HH21, expression was found in precursors of dorsal interneurons (A). Expression was also seen in the dorsal root ganglia (DRG). Expression of CD34 (D-F) was more ubiquitous with highest levels in DRG and increasing levels in motoneurons at HH25 (F).

Supplementary Figure 4

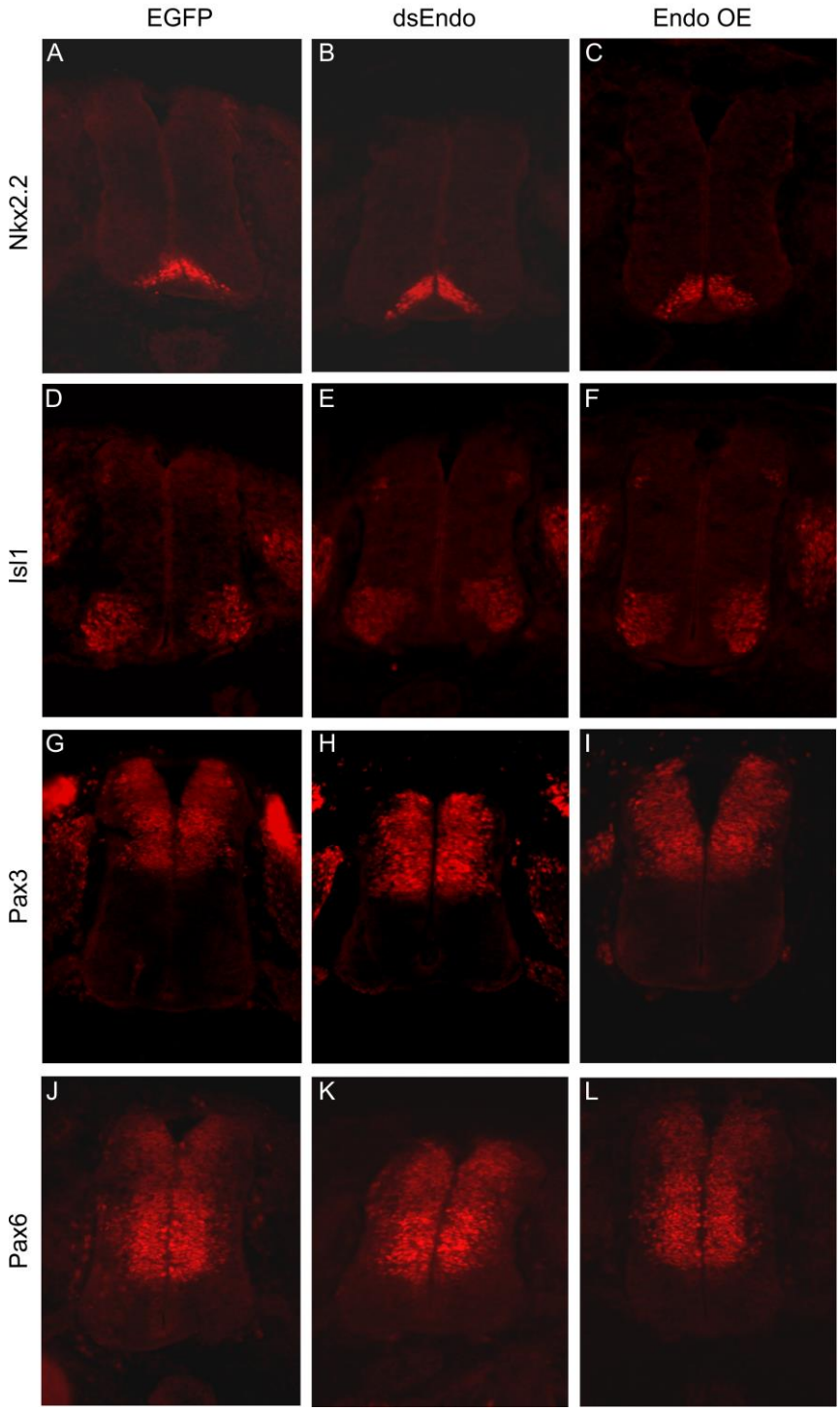

Supplementary Figure 4

Downregulation or overexpression of Endoglycan does not affect spinal cord patterning.

To check whether the effect of Endoglycan perturbation on axonal pathfinding was indirect due to changes in spinal cord patterning, we used a series of antibodies to stain sections taken from control embryos expressing

GFP (A,D,G,J), embryos electroporated with dsEndo (B,E,H,K), or embryos overexpressing Endoglycan (C,F,I,L). We found no evidence for aberrant patterning, when we compared sections stained with Nkx2.2 (A-C), Islet1 (D-F), Pax3 (G-I), or Pax6 (J-L).

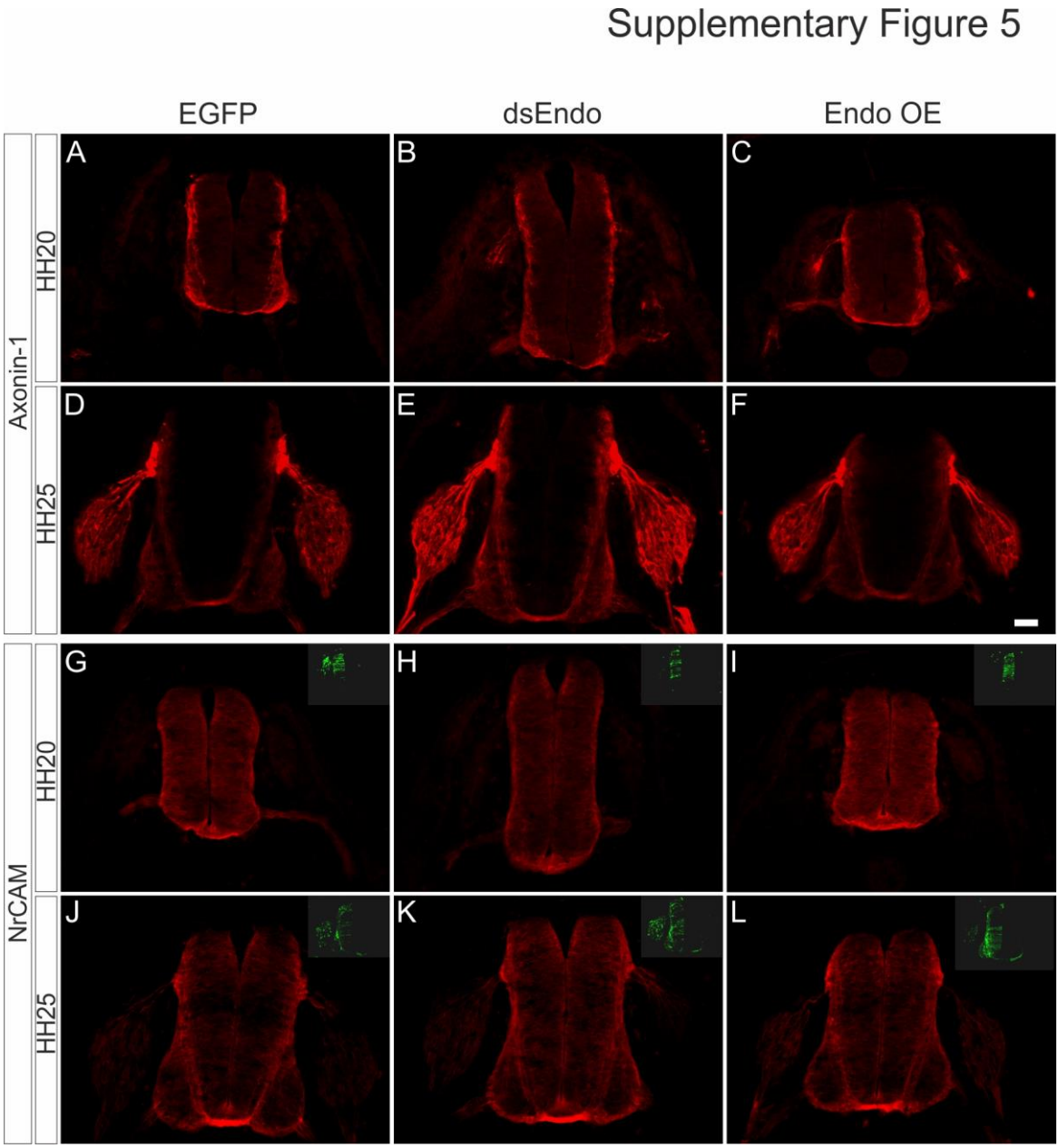

1080

1081 Supplementary Figure 5

1082 **The errors in commissural axon pathfinding seen after perturbation of Endoglycan levels are not due to**

1083 **changes in the expression of known guidance cues for dI1 axons**

1084 To exclude that the changes in axonal pathfinding seen after silencing or overexpression of Endoglycan were

1085 explained by an effect on the expression of known axon guidance cues for dI1 axons, Axonin-1/Contactin-2 (A-

1086 F) or NrCAM (G-L), we compared sections taken from control embryos electroporated with a plasmid encoding

1087 GFP (A,D,G,J), embryos electroporated with dsEndo (B,E,H,K), or embryos overexpressing Endoglycan (C,F,I,L).

1088 We found no differences in expression of Axonin-1 and NrCAM. We compared sections taken from embryos

1089 sacrificed at HH20 (A-C, G-I) and HH25 (D-F, J-L). Bar: 50 µm.

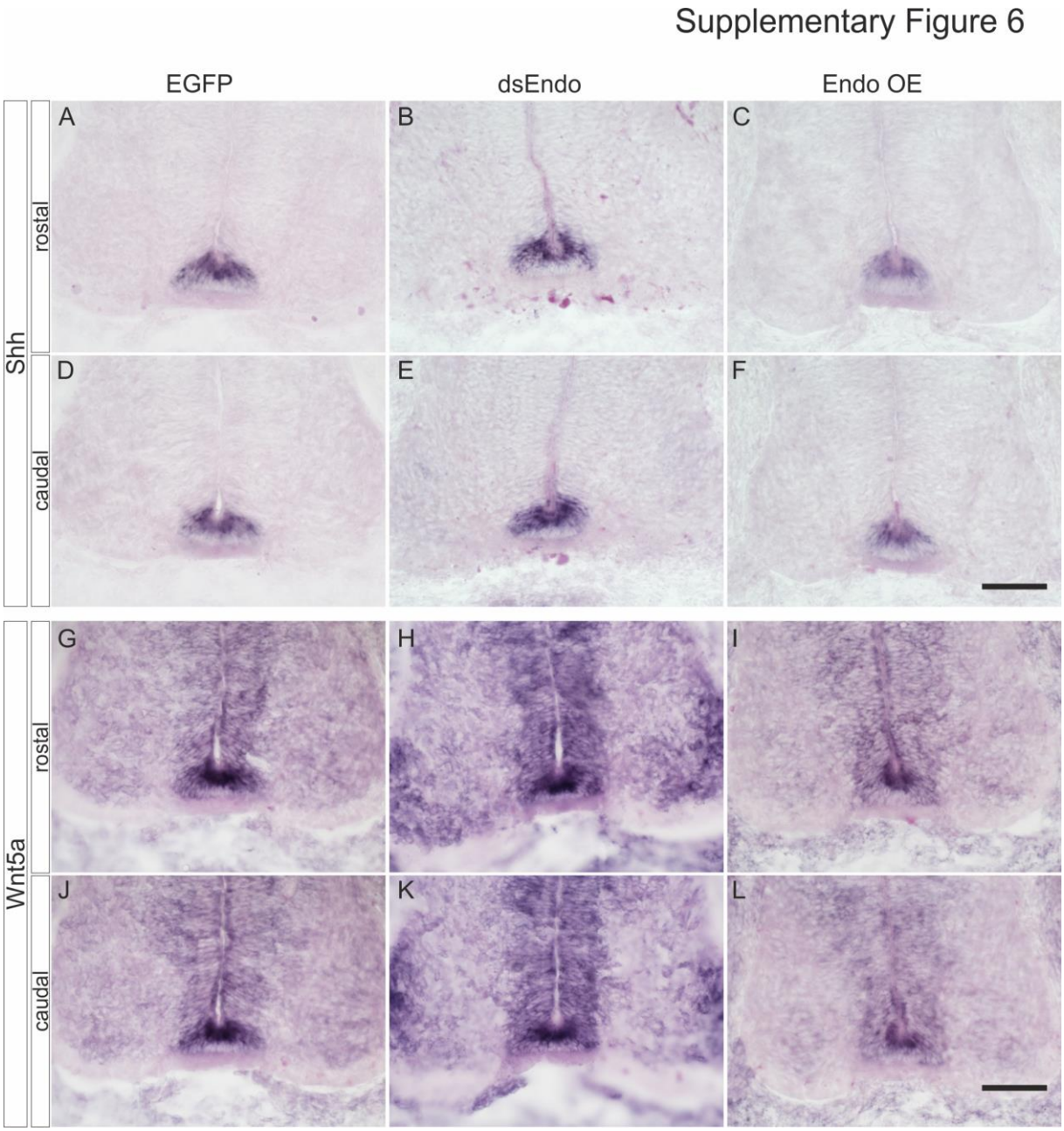

Supplementary Figure 6

Perturbation of Endoglycan expression does not affect guidance of post-crossing commissural axons indirectly by changing Shh or Wnt5a expression

We did not find any changes in the expression of *Shh* (A-F) or *Wnt5a* (G-L) compared to control embryos expressing EGFP (A,D,G,J) after silencing *Endoglycan* (B,E,H,K) or after overexpression of *Endoglycan* (C,F,I,L). *Shh* was found at higher levels in the caudal compared to the rostral floor plate (A-F), as reported previously (Bourikas et al., 2005). *Wnt5a* levels did not differ between rostral and caudal sections taken from the lumbar part of the spinal cord, as reported earlier (Domanitskaya et al., 2010).

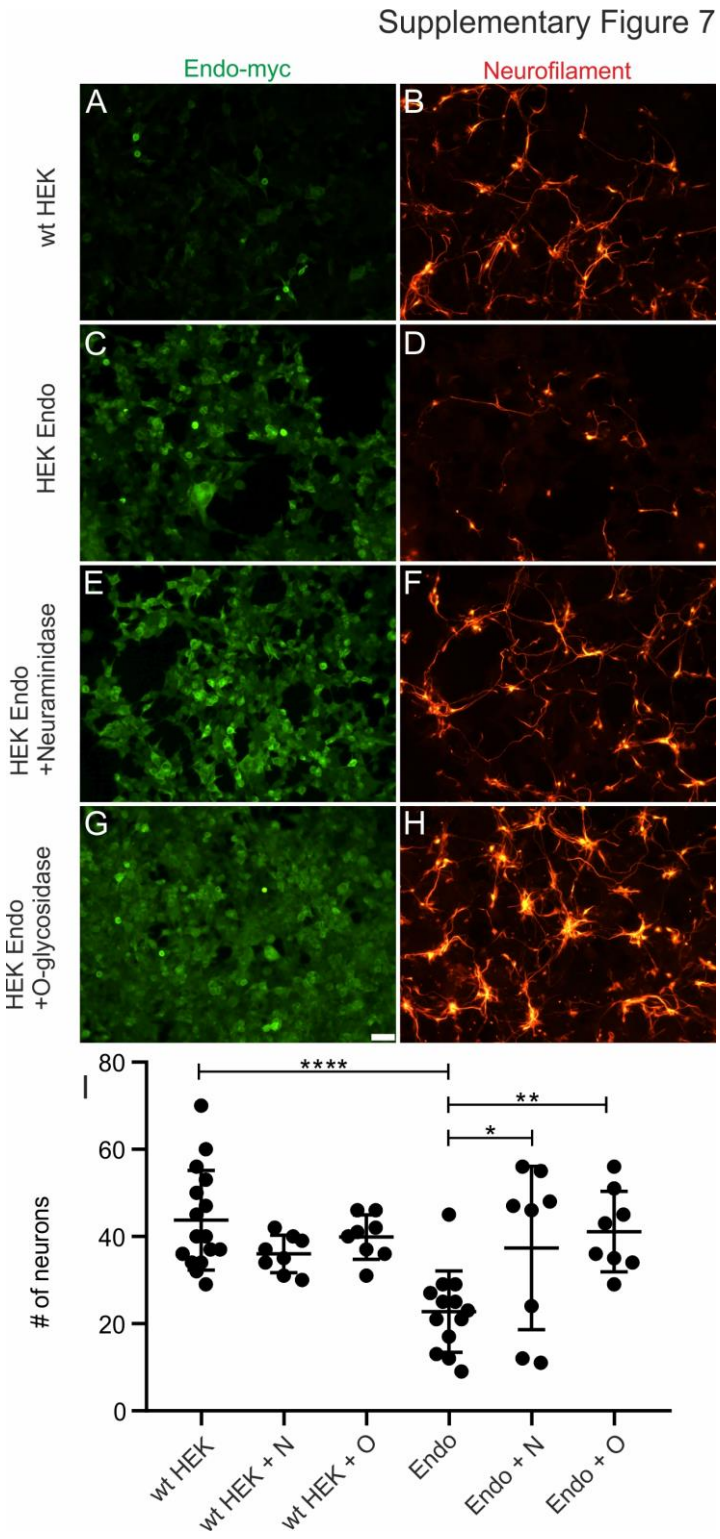

Supplementary Figure 7

Post-translational modification of Endoglycan is required for its anti-adhesive effects

Control HEK cells (A-B) or Endoglycan-expressing HEK cells (C-H) were plated as carpet for motoneurons (stained with anti-neurofilament antibodies in B,D,F,H). Before adding the motoneurons, HEK cells were either

1106 left untreated (A-D), or treated with neuraminidase (E,F) or O-glycosidase (G,H) for 2 hours. Attached
1107 motoneurons were counted after 40 hours. Removal of sialic acid by neuraminidase (E,F) or O-glycosidase (G,H)
1108 abolished the anti-adhesive effect of Endoglycan (C,D). Quantification of the number of attached motoneurons
1109 under the different conditions is shown in (I).

1110

1111

1112

Supplementary Figure 8

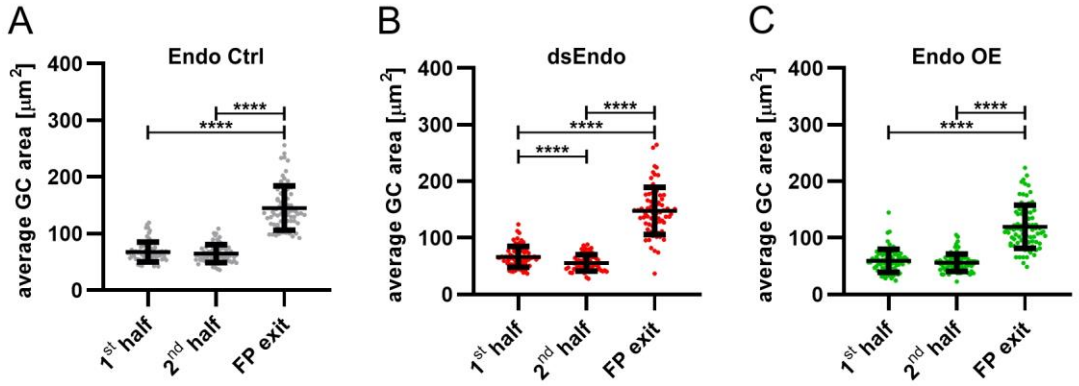

1113

1114 Supplementary Figure 8

1115 **Growth cone size is enlarged at the floor-plate exit site**

1116 Data at the single axon level extracted from 24h time-lapse recordings of dI1 axons crossing the floor plate. The
1117 average growth cone area was measured in the first half, the second half and at the exit site of the floor plate
1118 for each condition. (A) No difference in the area was detected between growth cones in the first half and the
1119 second half of the floor plate in controls. However, growth cones were found to be much enlarged at the exit
1120 site compared to when they were in the floor plate (Friedman test with Dunn's multiple-comparisons test). (B)
1121 Unilateral down regulation of Endoglycan induced a significant decrease in the average growth cone area in the
1122 second part of the floor plate compared to the first part. However, dI1 growth cones still got much larger when
1123 exiting the floor plate compared to when they were located in the floor plate (one-way RM ANOVA with Sidak's
1124 multiple-comparisons test). (C) After unilateral overexpression of Endoglycan, no difference in growth cone
1125 area was detected between the first and the second half of the floor plate. Like in all other conditions, they
1126 were found to be much enlarged at the exit site (Friedman test with Dunn's multiple-comparisons test). Error

1127 bars represent standard deviation. p<0.0001 (****), p<0.001 (***), p<0.01 (**), p<0.05 (*) and p≥0.05 (ns) for

1128 all tests. See Table 2 for detailed results.

1129

1130

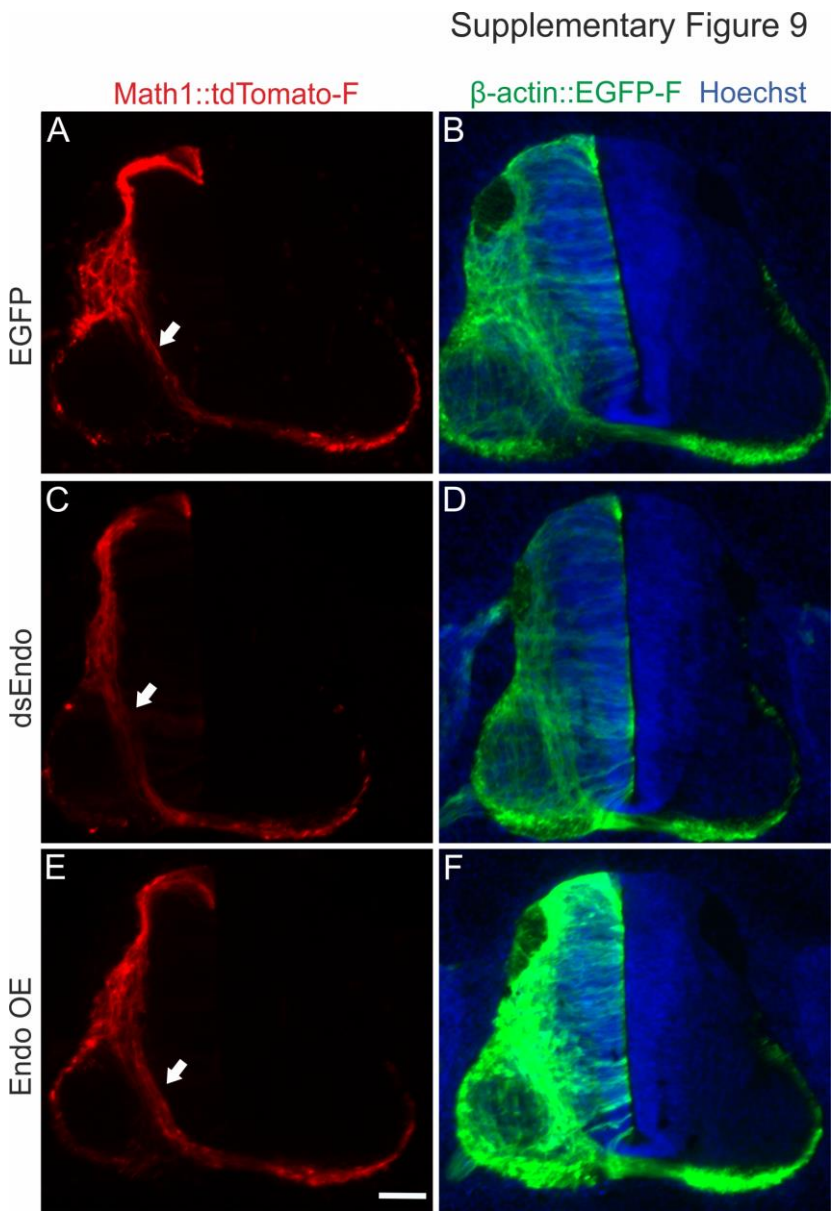

1131

1132

1133 Supplementary Figure 9

1134 **Endoglycan does not affect pre-crossing commissural axons**

1135 We found no differences in timing or trajectories of pre-crossing commissural axons labeled by the co-

1136 electroporation of Math1::tdTomato-F when we compared control embryos electroporated with an EGFP

1137 plasmid (A,B) with embryos electroporated with dsEndo (C,D) or embryos overexpressing Endoglycan (E,F).

Supplementary Figure 10

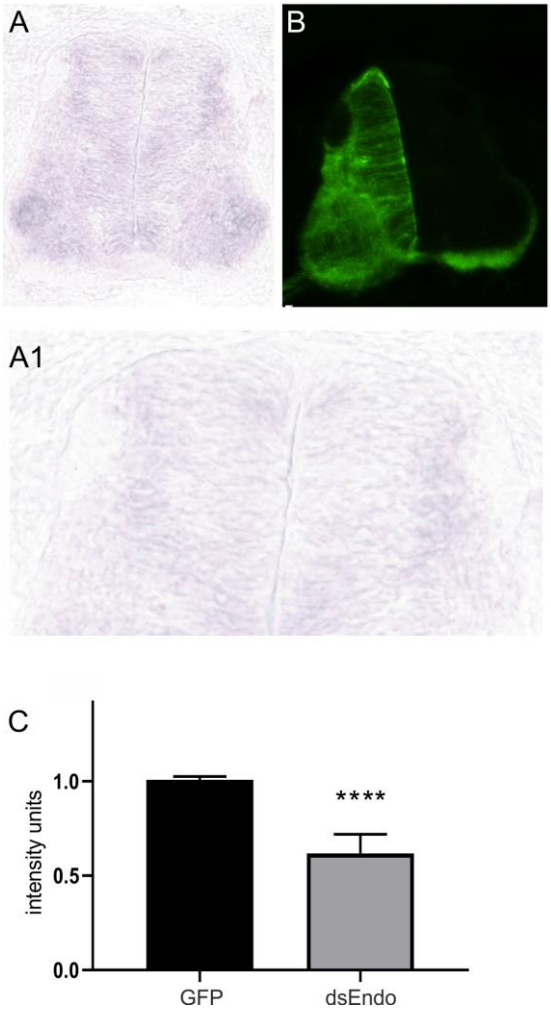

1138

1139

1140 Supplementary Figure 10

1141 **Electroporation of dsRNA derived from Endoglycan effectively downregulates Endoglycan mRNA**

1142 In the absence of antibodies detecting Endoglycan, we had to use in situ hybridization to quantify the efficiency
1143 of Endoglycan downregulation (A). When we compared expression levels of Endoglycan between the
1144 electroporated and the non-electroporated side of a HH25 spinal cord, we found reduced signal intensities on
1145 the electroporated side. (B) Co-electroporation of a plasmid encoding GFP together with dsEndo allows for the
1146 identification of the electroporated side. On average, electroporation of dsEndo reduced mRNA levels by 39%.
1147 Keep in mind that only about 50% of the cells in the electroporated area are taking up the dsRNA. Therefore,
1148 the reduction in Endoglycan is very efficient in the transfected cells. Three sections per embryo and three
1149 embryos per group were included in the analysis.

1150 **Legends to supplementary movies**

1151

1152

1153 Supplementary Movie 1

1154 24h time-lapse recordings of tdTomato-positive dI1 axons (shown in black) in control (Endo control),
1155 Endoglycan knockdown (dsEndo) and Endoglycan overexpression (Endo OE) conditions. Dashed lines represent
1156 floor plate boundaries. R, rostral; C, caudal.

1157

1158

1159 Supplementary Movie 2

1160 Representative examples of the floor plate crossing of tdTomato-positive dI1 axons (shown in black) taken from
1161 24h time-lapse recordings from control (Endo control), Endoglycan knockdown (dsEndo) and Endoglycan
1162 overexpression (Endo OE) conditions. An arrowhead in each condition points at the migrating growth cone.
1163 Dashed lines represent floor-plate boundaries.

1164

1165

1166 Supplementary Movie 3

1167 Example of a 24h time-lapse recordings of tdTomato-positive dI1 axons (shown in black) showing guidance
1168 defects at the exit site of the floor plate in Endoglycan overexpression condition. Stalling growth cones are
1169 shown by arrowheads and caudally turning growth cones by arrows. Rostral is up. Dashed line represents the
1170 floor-plate exit site.

1171

1172

1173 Supplementary Movie 4

1174 The trajectory of single dI1 axons in the first half of the floor plate (electroporated half) in the absence of
1175 Endoglycan was aberrant and showed a ´corkscrew´-like phenotype. Example of a tdTomato-positive dI1 axon
1176 taken from a 24h time-lapse recording of an 'Endoglycan-knockdown' spinal cord. Arrowheads show how the
1177 growth cone is migrating within the first half (electroporated half) of the floor plate and enter in contact with

1178 mislocated EGFP-positive cells (arrows) that induced a ´corkscrew´ like morphology of the shaft. The 3D coronal
1179 rotation clearly shows that the axon and cells are located within the commissure (arrowhead).
1180
1181
1182 Supplementary Movie 5
1183 The trajectory of single dI1 axons in the first half of the floor plate (electroporated half) in the absence of
1184 Endoglycan was aberrant and showed a ´corkscrew´-like phenotype. Example of tdTomato-farnesylated-
1185 positive dI1 axons taken from 24h time-lapse recordings of an 'Endoglycan-knockdown' spinal cord.
1186 Arrowheads show how two growth cones are migrating within the first half (electroporated half) of the floor
1187 plate. The first one made a loop within the floor-plate cell layer (arrowheads), as shown by the 3D coronal
1188 rotation. The second one was attracted towards mislocalized EGFP-positive cells (arrow), made contact with
1189 them and then carried out a U-turn toward them before continuing its migration in the direction of the midline.
1190 The 3D coronal view confirmed that the second growth cone during its U-turn and the mislocalized cells were
1191 located within the commissure (arrowhead).
1192 Table 1
1193 **The source of Endoglycan does not matter**
1194

Treatment	**No of embryos**	**No of inj. sites**	**% inj sites normal PT**	**P-value**
untreated	14	111	85.3 ± 2.6	0.999
GFP	14	85	80.5± 6.7	1
dsEndo	15	111	30.2±5.3	<0.0001
β-actin::EndoOE	16	91	49.1±2.2	0.0184
Hoxa1::Endo-L	25	234	38.5±5.7	<0.0001
Hoxa1::Endo-M	18	136	60.3±6.7	0.3403
Hoxa1::Endo-H	6	64	24.6±10.9	<0.0001

Math1::Endo-L	15	157	59.6±6.8	0.3515
Math1::Endo-M	7	86	35±10.7	0.0032
Math1::Endo-H	8	86	26.3±6.5	<0.0001

Concomitant expression of Endoglycan could rescue the aberrant axon guidance phenotype induced by the downregulation of Endoglycan throughout the spinal cord. It did not matter whether Endoglycan was expressed under the Hoxa1 enhancer for specific expression in floor-plate cells, or under the Math1 enhancer for specific expression in dI1 neurons. However, the rescue effect was dose-dependent. Too little, or too much Endoglycan was inducing axon guidance defects. For rescue, *Endoglycan* cDNA under the control of the Hoxa1 enhancer (Hoxa1::Endo) or the Math1 enhancer (Math1::Endo) were injected at 150 ng/µl (low, L), 300 ng/µl (medium, M), or 750 ng/µl (high, H). The number of embryos and the number of DiI injection sites analyzed per group are indicated. The average % of injection sites with normal axon guidance phenotypes and the P-value for the comparison between the respective group and the control-treated (EGFP-expressing) group are given.

Table 2

Quantification of midline crossing of dI1 axons using live imaging

Figure 7					
part	**name**	**value**	**stdev**	**n(axons)**	**N(embryos)**
B	Endo Ctrl	5.38	1.25	161	3
B	dsEndo	5.50	1.20	168	3
B	Endo OE	4.35	1.38	234	3
C	EndoCtrl Ent-Mid	2.74	0.94	161	3
C	Endo Ctrl Mid-Ex	2.64	1.01	161	3
C	dsEndo Ent-Mid	3.06	0.88	168	3
C	dsEndo Mid-Ex	2.45	1.02	168	3
C	Endo OE Ent-Mid	2.10	0.71	234	3
C	Endo OE Mid-Ex	2.26	0.83	234	3
D	Endo Ctrl	0.51	0.13	161	3
D	dsEndo	0.56	0.12	168	3
D	Endo OE	0.48	0.11	234	3
E	Endo Ctrl	0.49	0.13	161	3
E	dsEndo	0.44	0.12	168	3
E	Endo OE	0.52	0.11	234	3
F	Endo Ctrl	67.70	17.56	70	3
F	dsEndo	66.58	18.43	68	3
F	Endo OE	59.51	20.29	83	3

G	Endo Ctrl	64.91	15.84	70	3
G	dsEndo	55.91	14.27	68	3
G	Endo OE	56.20	15.29	83	3
H	Endo Ctrl	145.07	39.29	70	3
H	dsEndo	147.84	41.85	68	3
H	Endo OE	119.72	38.32	83	3
Supplementary Figure 8					
A	1st half	67.70	17.56	70	3
A	2nd half	64.91	15.84	70	3
A	FP exit	145.07	39.29	70	3
B	1st half	66.58	18.43	68	3
B	2nd half	55.91	14.27	68	3
B	FP exit	147.84	41.85	68	3
C	1st half	59.51	20.29	83	3
C	2nd half	56.20	15.29	83	3
C	FP exit	119.72	38.32	83	3

The table contains the detailed values from results presented in Figure 7 and Supplementary Figure 8. Ent, entry; Mid, midline; Ex, exit; FP, floor plate; stdev, standard deviation.